



## Article

# NOAA MODIS SST Reanalysis Version 1

Olafur Jonasson <sup>1,2,\*</sup>, Alexander Ignatov <sup>1</sup>, Boris Petrenko <sup>1,2</sup>, Victor Pryamitsyn <sup>1,2</sup>  and Yury Kihai <sup>1,2</sup>

<sup>1</sup> STAR, NOAA Center For Weather and Climate Prediction (NCWCP), College Park, MD 20740, USA; alex.ignatov@noaa.gov (A.I.); boris.petrenko@noaa.gov (B.P.); victor.pryamitsyn@noaa.gov (V.P.); yury.kihai@noaa.gov (Y.K.)

<sup>2</sup> Global Science and Technology, Inc., Greenbelt, MD 20770, USA

\* Correspondence: olafur.jonasson@noaa.gov

**Abstract:** The first NOAA full-mission reanalysis (RAN1) of the sea surface temperature (SST) from the two Moderate Resolution Imaging Spectroradiometers (MODIS) onboard Terra (24 February 2000–present) and Aqua (4 July 2002–present) was performed. The dataset was produced using the NOAA Advanced Clear-Sky Processor for Ocean (ACSP) enterprise SST system from Collection 6.1 brightness temperatures (BTs) in three MODIS thermal emissive bands centered at 3.7, 11, and 12  $\mu\text{m}$  with a spatial resolution of 1 km at nadir. In the initial stages of reprocessing, several instabilities in the MODIS SST time series were observed. In particular, Terra SSTs and corresponding BTs showed three ‘steps’: two on 30 October 2000 and 2 July 2001 (due to changes in the MODIS operating mode) and one on 25 April 2020 (due to a change in its nominal blackbody temperature, BBT, from 290 to 285 K). Additionally, spikes up to several tenths of a kelvin were observed during the quarterly warm-up/cool-down (WUCD) exercises, when the Terra MODIS BBT was varied. Systematic gradual drifts of  $\sim 0.025$  K/decade were also seen in both Aqua and Terra SSTs over their full missions due to drifting BTs. These calibration instabilities were mitigated by debiasing MODIS BTs using the time series of observed minus modeled (‘O–M’) BTs. The RAN1 dataset was evaluated via comparisons with various in situ SSTs. The data meet the NOAA specifications for accuracy ( $\pm 0.2$  K) and precision (0.6 K), often by a wide margin, in a clear-sky ocean domain of 19–21%. The long-term SST drift is typically less than 0.01 K/decade for all MODIS SSTs, except for the daytime ‘subskin’ SST, for which the drift is  $\sim 0.02$  K/decade. The MODIS RAN1 dataset is archived at NOAA CoastWatch and updated monthly in a delayed mode with a latency of two months. Additional archival with NASA JPL PO.DAAC is being discussed.



**Citation:** Jonasson, O.; Ignatov, A.; Petrenko, B.; Pryamitsyn, V.; Kihai, Y. NOAA MODIS SST Reanalysis

Version 1. *Remote Sens.* **2023**, *15*, 5589. <https://doi.org/10.3390/rs15235589>

Academic Editor: Dongdong Wang

Received: 27 September 2023

Revised: 21 November 2023

Accepted: 27 November 2023

Published: 30 November 2023



**Copyright:** © 2023 by the authors. Licensee MDPI, Basel, Switzerland. This article is an open access article distributed under the terms and conditions of the Creative Commons Attribution (CC BY) license (<https://creativecommons.org/licenses/by/4.0/>).

**Keywords:** NOAA; ACSP; sea surface temperature; SST; MODIS; NLSST; VIIRS; AVHRR; Aqua; Terra; reanalysis; RAN1; stability; CRTM; radiative transfer; clear-sky mask

## 1. Introduction

The Advanced Clear-Sky Processor for Ocean (ACSP; see the abbreviations at the end of this paper) sea surface temperature (SST) enterprise system, designed and maintained at NOAA, provides SSTs from multiple satellites in geostationary (GEO) and low Earth orbits (LEO). Full-mission reprocessed high-resolution ( $\sim 1$  km or higher at nadir) ACSP SST data from VIIRS (flown onboard afternoon orbit ‘PM’ satellites NPP, N20 and N21) and AVHRR FRAC (flown onboard mid-morning orbit ‘AM’ satellites Metop-A, B and C) are publicly available [1,2]. The ACSP VIIRS SST dataset extends back to February 2012 (earliest NPP SST data), and AVHRR FRAC SST is available back to December 2006 (earliest Metop-A SST data).

This work documents the first ACSP SST Reanalysis (RAN1) dataset produced from two Moderate Resolution Imaging Spectroradiometers (MODIS). The first MODIS was launched on 18 December 1999 onboard the Terra satellite, and the second was launched on 4 May 2002 onboard the Aqua satellite. The MODIS RAN1 SSTs go back to the earliest available high-quality MODIS Brightness Temperatures (BTs) in the thermal emissive

bands (TEBs) (24 February 2000 for Terra and 4 July 2002 for Aqua). Data from Collection 6.1 L1b are used [3,4]. As of the time of writing, both MODIS sensors remain active, with the RAN1 data updated monthly in a delayed mode with an approximately two-month latency [5]. The over two-decade, continuous, long-term time series of high-resolution SST data make the MODIS record unique. No other currently available high-resolution satellite SST dataset matches the longevity, consistency, and quality of Aqua and Terra. Similar to its predecessor, AVHRR, and successor, VIIRS, MODIS is an Earth-viewing, cross-track-scanning instrument. Of its 36 spectral bands, covering from 0.4 to 14.4  $\mu\text{m}$ , three mid-wave infrared bands (MWIR; bands 20, 22, and 23) and three long-wave infrared bands (LWIR; bands 29, 31 and 32), all with a 1 km resolution at nadir, are positioned in three atmospheric windows and are suitable for SST retrieval.

The MODIS RAN1 dataset is produced in L2P (original swath projection), L3U ( $0.02^\circ$  gridded uncollated), and L3C ( $0.02^\circ$  gridded collated) formats. All products are compliant with the Group for High-Resolution SST (GHRSSST) Data Specification v2 (GDS2) standard [6]. As of the time of writing, a full archive of Aqua and Terra L3C data is available at NOAA CoastWatch [5]. Archival of the full L2P, L3U, and L3C records at JPL PO.DAAC is being explored. The L2P data are reported in 10 min granules (144 files/24 h) with a  $\sim 950$  GB/year/satellite data volume. The  $0.02^\circ$  L3U data are produced from L2P files and reported in same-size 10 min granules (144 files/24 h), with a  $\sim 130$  GB/year/satellite data volume. The  $0.02^\circ$  L3C data are produced by collating L3U SST data from multiple satellite overpasses and reported in two files/24 h, one for day and one for night, with  $\sim 125$  GB/year/satellite data volume. Only data of the highest quality level, QL = 5 (classified as 'clear-sky' by the ACSPO Clear-Sky Mask, ACSM [7]) are recommended for use. All evaluations of the MODIS RAN1 dataset in this study are based on L2P data. The performance of the L3U and L3C SST products (in terms of global mean bias and standard deviation against in situ SSTs, and coverage) is comparable or superior to that of L2P, and therefore, their evaluation is omitted here in the interest of space.

Note that ACSPO MODIS RAN1 is not the first or only full-mission reprocessed MODIS SST dataset. The other dataset available at the time of writing is the NASA R2019 SST, which is also based on MODIS Collection 6.1 L1b data. The previous version, R2014, was documented in [8], with R2019 updates summarized in [9]. The NASA R2019 SST dataset is available in L2P format and in various flavors of L3 (including daily, weekly, monthly and annual averages) at spatial resolutions of 4.63 km and 9.26 km [10,11]. The NASA R2019 L2P dataset will be discussed later in this work, to place the performance of the ACSPO RAN1 SST in context. Standard metrics, such as the accuracy (global mean bias with respect to quality-controlled in situ data from drifters and tropical moorings, DTMs), precision (corresponding standard deviation), and the relative size of their clear-sky domains are evaluated. Sensitivity to true SST is another important metric of SST performance [12,13]. RAN1 sensitivities are discussed later in this work. The sensitivity of the NASA SST is unknown to us, and this metric cannot be compared with the ACSPO. Comparisons with ACSPO VIIRS SSTs [1] will also be performed where appropriate. The primary motivation for producing the MODIS RAN1 dataset with the NOAA ACSPO system was to facilitate its inclusion in the NOAA multi-sensor L3S-LEO high-resolution SST product, which currently only includes data from JPSS VIIRSs and Metop-FG AVHRR FRACs [1,2,14]. NOAA users have expressed interest in including MODIS in the L3S-LEO and extending its time series back to 2000.

This work is organized as follows: Section 2 discusses the Terra and Aqua orbits. Section 3 provides an overview of the ACSPO MODIS algorithms with emphasis on SST retrievals and a comparison with the ACSPO VIIRS and AVHRR algorithms. Section 4 validates MODIS SSTs against iQuam in situ SSTs from drifting and tropical moored buoys (DTMs) with complementary validation against Argo floats (AFs) presented in Appendix A [15]. Section 5 documents the mitigation/debiasing of residual calibration artifacts in the MODIS TEBs, including discontinuities and drifts of BTs in individual bands. The debiasing is performed using comparisons of observed MODIS BTs with modeled

BTs, obtained using the NOAA Community Radiative Transfer Model (CRTM) [16–18]. Section 6 summarizes the results of this study and discusses future work.

## 2. Terra and Aqua Orbits

The Aqua and Terra spacecraft fly in Sun-synchronous orbits at lower altitudes compared to the JPSS satellites (~705 vs. ~824 km) with nominal local equator crossing times: LEXT~1:30 a.m./p.m. for Aqua and 10:30 a.m./p.m. for Terra. The higher JPSS orbits, combined with the wider  $\pm 56.28^\circ$  Earth-view sector compared with  $\pm 55.28^\circ$  for MODIS, result in a wider ~3060 km VIIRS swath, compared with the ~2330 km swath for MODIS [19,20]. As a result, VIIRS provides full global daily coverage of the Earth, whereas consecutive MODIS overpasses may not overlap, leaving some data voids near the equator. While fuel remained, the Aqua and Terra LEXTs have been maintained in a stable state throughout their lifetimes via regular spacecraft maneuvers.

Figure 1 shows time series of the  $\Delta$ LEXT (actual LEXTs minus their nominal 1:30 and 10:30 values) for Aqua and Terra and compares them with the current NOAA JPSS series. The LEXT of the ascending node is close to 1:30 p.m. for the afternoon Aqua, NPP, and N20, and it is close to 10:30 p.m. for the mid-morning Terra. Figure 1 shows that the actual Aqua LEXT was  $1:35 \pm 0.05$  a.m./p.m. until it ran out of fuel and its orbit started drifting following the last orbit correction maneuver in March 2021. As of May 2023, the Aqua LEXT has drifted to ~1:45 a.m./p.m. The Terra LEXT was 10:45 a.m./p.m. immediately after launch, but then allowed to drift to 10:30 a.m./p.m. over the course of its first two years, and maintained in a stable state until its last orbit maintenance maneuver in February 2020. Terra is also out of fuel now, and as of May 2023, the Terra LEXT had drifted to ~10:10 a.m./p.m. If a stable local time of SST observations is critical for users, then caution should be exercised when using Aqua SSTs after March 2021 and Terra SSTs before January 2002 and after February 2020.

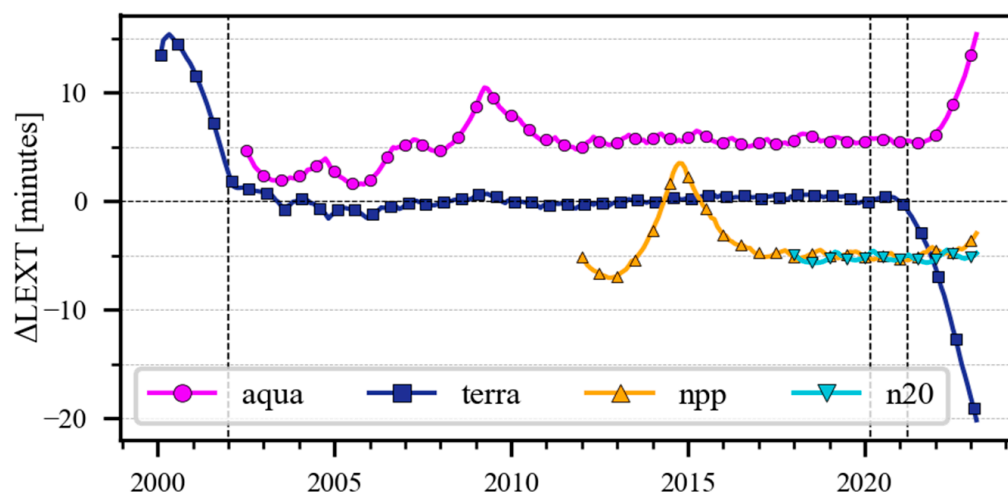


**Figure 1.** Time series of the  $\Delta$ LEXT (delta between the actual satellite LEXTs and their nominal 1:30 a.m./p.m. and 10:30 a.m./p.m. values). The three vertical dotted lines mark key dates: 1 January 2002 (approximate end of the Terra LEXT drift from 10:45 to 10:30 a.m./p.m.) and 27 February 2020/18 March 2021 (last Terra/Aqua orbit correction maneuvers). Note that the monthly mean (on the first day of the month; shown by symbols) LEXTs are calculated using the ‘pyorbital’ python package [21] as the average of all ascending nodes in a day using two line elements (TLEs) from [celestrak.com](http://celestrak.com) (accessed on 17 May 2023).

For comparison, the NPP LEXTs fluctuated between 1:23 and 1:33 prior to 2017, and then maintained at  $1:25 \pm 0.02$  a.m./p.m. since 2017. N20 has been maintained in a consistent orbit with a LEXT of  $\sim 1:25 \pm 0.01$  a.m./p.m. The close proximity between the Aqua, NPP, and N20 LEXTs greatly facilitates the inclusion of the Aqua SST in the ACSPO L3S-LEO-PM product, which previously included only NPP and N20 [14]. We also plan to

include N21 later in 2023. Both the Aqua and Terra SSTs have been included in the ACSPO daily L3S-LEO-DY SST product, which is reported once per 24 h with the diurnal SST variation normalized at 1:30 a.m. local-time viewing conditions [14]. Prior to the addition of MODIS and N21 VIIRS, the L3S-LEO-DY was based on daytime and nighttime SSTs from three AVHRR FRACs flown onboard Metop-A/B/C and two VIIRSs onboard the NPP/N20 satellites.

### 3. ACSPO Algorithms

In ACSPO, the SST is retrieved from clear-sky BTs in MODIS bands 20, 31, and 32, centered at 3.7, 11, and 12  $\mu\text{m}$ , respectively. During the daytime (pixels with solar zenith angle  $\leq 90^\circ$ ), two reflective solar bands (1 and 2) centered at 0.65 and 0.86  $\mu\text{m}$  are additionally used by the ACSM [7].

The ACSPO files report the ‘subskin’ SST (often considered a proxy for temperature at a  $\sim 1$  mm depth) in the ‘sea\_surface\_temperature’ variable. Note that satellite infrared radiometers are sensitive to skin SST (effective temperature of the top  $\sim 10$   $\mu\text{m}$  layer), which is typically several tenths of a kelvin colder than the subskin SST due to radiative losses at the ocean surface [6]. Since skin SSTs available from shipborne infrared radiometers are very scarce and insufficient for the calibration and validation of satellite SSTs, satellite retrievals are often trained against much more numerous conventional in situ SSTs measured by drifting and tropical moored buoys (DTMs), typically using sampling temperatures at  $\sim 20$  cm to  $\sim 1$  m depths. Some data producers (e.g., [8,9]) subtract 0.17 K (the mean cold skin effect) from the derived SSTs and call their products ‘skin’ SST. (Note that this offset should be added back when ‘skin’ SSTs are validated against the same DTM data to ensure an expected zero bias). Other SST groups, including OSISAF [22] and ACSPO, do not subtract the 0.17 K and call their products ‘subskin’ (saving the need to add this offset back at the validation stage). The ‘skin’ and ‘subskin’ terms are thus merely two different conventions that are currently in use. To emphasize this fact, they are bracketed with quote/unquote symbols in the remainder of the paper.

In compliance with the GDS2 standard [6], ACSPO files also report two sensor specific error statistics (SSES) variables for each pixel, bias and standard deviation, which are estimated vs. DTM SSTs. Subtracting the SSES bias (stored in the ‘sses\_bias’ variable) from the ‘subskin’ SST gives the ACSPO ‘depth’ SST (another convention, adopted in the ACSPO products), a better proxy for the SST at depths of  $\sim 0.2$ – $1.0$  m typically sampled by DTMs. Both the ACSPO ‘subskin’ and ‘depth’ SSTs are calculated using the nonlinear SST (NLSST) equation [12,23]. The main difference between the two is that the ‘subskin’ SST is calculated using a global regression algorithm (with only two sets of regression coefficients, one set for night and another set for day). In contrast, the ‘depth’ SST is calculated using a piecewise regression algorithm, where the retrieval domain is stratified into multiple segments, each with its own regression coefficients [24]. Owing to segmentation of the retrieval domain and the larger number of trainable parameters, the piecewise regression SST agrees more closely with the DTM SSTs (cf. Section 4). However, as discussed later in this section, its retrieval sensitivity is considerably lower than that for global regression due to the significant contribution from prior information, such as the first-guess SST, resulting in reduced spatial and temporal SST gradients [12,13].

At night (pixels with solar zenith angle  $> 90^\circ$ ), the SST is retrieved using a three-band equation of the following form:

$$T_S = a_0 + a_1 T_{11} + a_2 (T_{11} - T_{3.7}) + a_3 (T_{11} - T_{12}) + a_4 T_{11} S + a_5 (T_{11} - T_{3.7}) S + a_6 (T_{11} - T_{12}) S + a_7 (T_{11} - T_{3.7}) T_0 + a_8 (T_{11} - T_{12}) T_0 + a_9 S + a_{10} \theta. \quad (1)$$

Here,  $T_{3.7}$ ,  $T_{11}$ , and  $T_{12}$  are MODIS BTs in bands centered at 3.7, 11, and 12  $\mu\text{m}$ ,  $S = \sec(\theta) - 1$ , and  $\theta$  is the satellite view zenith angle (VZA). During the daytime, the same equation is used, except that the terms with the 3.7  $\mu\text{m}$  BTs,  $T_{3.7}$ , are excluded due to contamination from reflected and scattered solar radiation:

$$T_S = b_0 + b_1 T_{11} + b_2(T_{11} - T_{12}) + b_3 T_{11} S + b_4(T_{11} - T_{12}) S + b_5(T_{11} - T_{12}) T_0 + b_6 S + b_7 \theta. \quad (2)$$

For MODIS, the VZA range is  $\pm 65^\circ$  with the convention that the VZA is positive at the beginning of the scan and negative at its end. The regression coefficients  $a_i$  and  $b_i$  have been trained using five years (2016–2021) of MODIS BTs matched with iQuam DTM SSTs. The regression coefficients are ‘static’ (i.e., calculated only once and used throughout the full Aqua and Terra missions). This is in contrast to ‘variable’ coefficients (e.g., those employed in ACSPO AVHRR FRAC RAN1 [2]), which are recalculated daily.

Table 1 lists the contributions (loads) of each MODIS band to the ‘subskin’ SST calculated using Equations (1) and (2). The individual band loads are defined as global mean partial derivatives of NLSST Equations (1) and (2) with respect to the BTs in each band. Table 1 shows that, for both night and day, the sum of the BT loads is close to one, as expected. At night, transparent band 20 centered at  $3.7 \mu\text{m}$  is the main contributor to the MODIS SST with mean loads of  $+1.30/+1.35$  for Terra/Aqua, respectively. The longwave split-window bands contribute much less, with weights of  $+0.34/+0.37$  for  $T_{12}$  (suggesting that this band does help with atmospheric correction) and only  $-0.02/-0.06$  for  $T_{11}$  (suggesting that this band contributes only minimally). During the daytime, the loads on the split-window bands are much larger,  $\sim +4$  for  $T_{11}$  and  $\sim -3$  for  $T_{12}$ , suggesting that, in the absence of the transparent  $3.7 \mu\text{m}$  band, both LWIR bands are essential for atmospheric correction. A side effect of the large contribution of the BT difference term is the amplification of noise present in BTs, which propagates into the retrieved SST [25]. In all ACSPO SST products from LEO satellites, noise in the BT difference terms is mitigated using a special smoothing algorithm, which extracts the ‘SST-correlated component’ from the BT differences and smooths only this ‘residual’ to prevent the smoothing of real SST features [26].

**Table 1.** Loads (global mean partial derivatives of Equations (1) and (2)) with respect to the BTs ( $T_\lambda$ ) and first-guess SST ( $T_0$ ). The corresponding standard deviations (SDs) are also shown. The results are shown for nighttime Equation (1), and daytime Equation (2). The global mean sensitivities of the satellite SSTs to the true SST and their standard deviations are also shown. The data were compiled from global Aqua and Terra data for the full year of 2016.

		$T_{3.7}$	$T_{11}$	$T_{12}$	$T_0$	Sensitivity
Night	Mean (Aqua)	+1.354	+0.017	−0.371	+0.005	0.967
	Mean (Terra)	+1.301	+0.057	−0.343	+0.000	0.973
	SD (Aqua)	0.142	0.427	0.288	0.012	0.016
	SD (Terra)	0.047	0.206	0.150	0.003	0.014
Day	Mean (Aqua)	-	+3.965	−2.997	+0.122	0.926
	Mean (Terra)	-	+3.999	−3.037	+0.114	0.922
	SD (Aqua)	-	0.887	0.886	0.058	0.054
	SD (Terra)	-	0.889	0.888	0.055	0.052

The larger loads on the LWIR bands in the daytime retrievals make them more sensitive to band-specific calibration drifts. In Section 5, we use the magnitudes and signs of individual BT loads to link the drift in retrieved SST to drifts in individual BTs.

An important metric for SST retrieval algorithms is the sensitivity of the retrieved SST to the true SST [12,13]. This is obtained by differentiating Equations (1) and (2) with respect to the SST, with the partial derivatives of BTs computed using CRTM [16–18]). Ideally, the sensitivity should be close to 1, uniform in space, and stable over time. Lower sensitivity values indicate a reduced ability to resolve spatial gradients and temporal variations in the retrieved SST. Table 1 lists the global mean ACSPO MODIS ‘subskin’ SST sensitivities to the true SST and the corresponding global standard deviations. The mean sensitivities are very consistent between Aqua and Terra, with a higher sensitivity at night ( $0.970 \pm 0.003$ ) and lower during the day ( $0.924 \pm 0.002$ ). The corresponding standard deviations are

$0.015 \pm 0.001$  at night and  $0.053 \pm 0.001$  during the daytime. Figure 2 shows the global distribution of the day- and nighttime sensitivities. The daytime sensitivity shows more spatial variability with lower values found in humid regions. The nighttime sensitivity is closer to 1 and is more spatially uniform due to the use of the atmospherically transparent MWIR band 20. Both MODIS sensitivities are slightly lower than for VIIRS ( $\sim 0.99$  for night and  $0.96$  for daytime [1]). This is likely due to the use of the LWIR M14 band centered at  $8.6 \mu\text{m}$  for VIIRS retrievals, whereas for MODIS, this band is unusable [1,27,28]. Table 1 also lists the load on the first-guess SST (i.e., the partial derivative of Equations (1) and (2) with respect to  $T_0$ ). The contribution of the first-guess SST is minimal at night ( $<0.01$ ) and moderate during the daytime ( $0.11$ – $0.12$ ). Recall that the linear Multi-Channel SST (MCSST) is often used at night due to the availability of the very transparent  $3.7 \mu\text{m}$  band [13]. During the daytime, the NLSST formulation is essential and a higher sensitivity to the first-guess SST is expected.

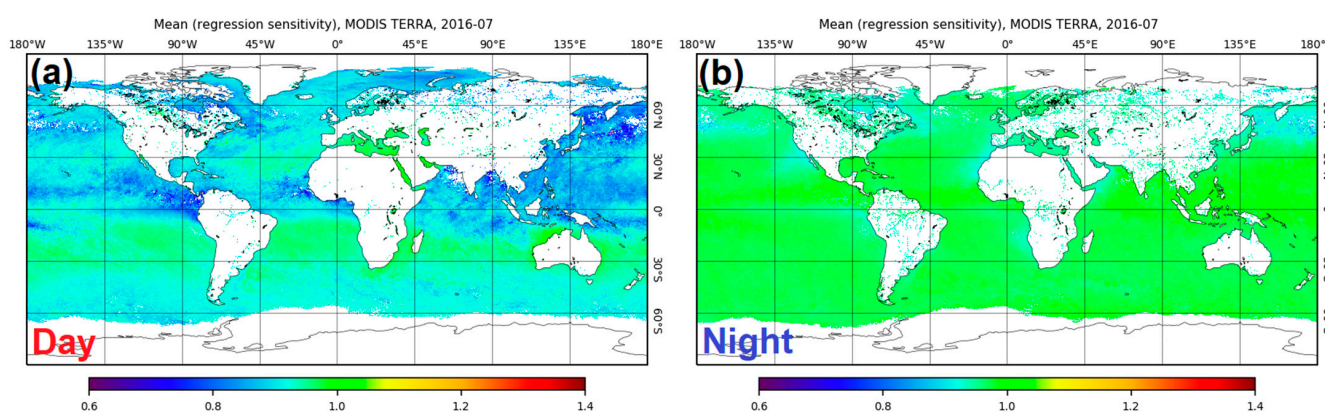


**Figure 2.** Monthly (June 2016)  $0.1^\circ$  aggregated maps of the mean sensitivity in ACSPO v2.80 Terra MODIS (a) daytime and (b) nighttime ‘subskin’ SSTs. During this time of year, the Northern Hemisphere atmosphere is warmer and moister compared to that of the Southern Hemisphere, resulting in a noticeably lower sensitivity north of the equator for the daytime SST. At night, the sensitivity is more uniform and closer to 1 due to the use of the more transparent MWIR band 20 centered at  $3.7 \mu\text{m}$ .

Equations (1) and (2) are the same as those used for ACSPO AVHRR FRAC SST retrievals [2], except for the last term that is proportional to the VZA ( $\theta$ ), which is not present in the ACSPO FRAC or VIIRS SST algorithms [1,2]. This is the only term in Equations (1) and (2) that is not symmetrical with respect to nadir. The reason for its inclusion in MODIS SST retrievals is historical. Early in the Terra MODIS mission, significant response versus scan angle (RVS) biases caused by the angular dependence of the MODIS scan mirror reflectivity were discovered in the LWIR bands [29]. The RVS issue resulted in large ( $\sim 2 \text{ K}$ ) SST biases across the Terra MODIS scan [8]. The RVS issue was addressed in MODIS Collection 3, with further refinements in later collections. MODIS RAN1 uses Collection 6.1 L1b data [3,4]. We found that the contribution of the VZA term to the SST is small for both Terra and Aqua ( $<0.01 \text{ K}$  at night and  $<0.10 \text{ K}$  during the daytime).

Equations (1) and (2) also differ from the VIIRS SST algorithm in that MODIS band 29 (centered at  $8.6 \mu\text{m}$ ) is not used due to its degraded performance (electronic crosstalk in both Aqua and Terra MODISs [1,27,28]). The absence of the  $8.6 \mu\text{m}$  band results in a slightly degraded quality for the MODIS SST compared to the VIIRS in terms of the precision (standard deviation with respect to the in situ SST; see Section 4) and a lower sensitivity to the true SST. The degradation of both the precision and sensitivity is more pronounced during the daytime, when atmospherically transparent MWIR bands cannot be used for SST retrievals.

ACSPO v2.80 ‘depth’ SSTs are calculated using the same Equations (1) and (2), except a piecewise regression algorithm is employed where the retrieval domain is split into multiple segments, with each segment having its own set of regression coefficients,  $a_i$  and

$b_i$  [24]. In ACSPO files, the ‘depth’ SST can be obtained by subtracting the ‘sres\_bias’ from the ‘sea\_surface\_temperature’. As will be shown in Section 4, the precision (global standard deviation with respect to in situ SST) is considerably improved for ‘depth’ compared to the ‘subskin’ SST. However, this comes at the price of a lower sensitivity. The global mean ACSPO MODIS night/day ‘depth’ SST sensitivity is only  $\sim 0.70/0.65$ , compared to  $\sim 0.97/0.92$  for the ‘subskin’ SST. Validation of both the ACSPO ‘subskin’ and ‘depth’ SSTs against various in situ SSTs from the iQuam online system [15] is presented in Section 4.

The ACSPO and NASA MODIS systems both employ regression SST algorithms, stratified by day and night, but with several substantial differences [8–11]. First, ACSPO produces ‘subskin’ SSTs in which the regressions are trained against in situ data (separately for day and night) and then employed in retrievals as-is (i.e., with no changes to the derived coefficients). In contrast, NASA produces the ‘skin’ SST, which is trained against in situ data similarly to ACSPO, but the regression offset is then adjusted by  $-0.17$  K, before making retrievals. The second difference is that ACSPO ‘subskin’ SSTs are derived using only one global set of regression coefficients for day, and one for night. In contrast, the NASA regression employed in R2019, is additionally stratified by month-of-the-year and seven latitudinal bands (below  $40^\circ\text{S}$ , four  $20^\circ$ -wide bands from  $40^\circ\text{S}$  to  $40^\circ\text{N}$ , one band between  $40^\circ\text{N}$  and  $60^\circ\text{N}$ , and one band for arctic regions above  $60^\circ\text{N}$ ) [8,9]. The monthly segmentation is performed only once (with the exception of the early Terra period) and used for subsequent years. The specific forms of the regressions also differ. The daytime regressions are most similar, both employing split-window NLSSTs with two LWIR bands, 31 and 32, centered at 11 and 12  $\mu\text{m}$ . At night, the ACSPO SST employs a three-band NLSST Equation (1) with one MWIR (20) and two LWIR bands (31 and 32) [1,2]. NASA, on the other hand, reports two products: SST (produced with the same daytime split-window LWIR NLSST, for consistency with the daytime retrievals), and a MODIS-unique SST4 (produced with the MWIR-only split-band algorithm, using bands 22 and 23 centered at 3.9 and 4.0  $\mu\text{m}$ ). Our additional analyses (not shown here) suggest, consistently with analyses performed by the R2019 producers, that the precision of the MWIR SST4 is considerably improved over that of the LWIR SST [8]. Section 4 consistently compares NASA and ACSPO SST validation metrics, including the accuracy, precision, and clear-sky ratio (but excluding the sensitivity, which was not available to us from the R2019).

The ACSM is a crucial component of the ACSPO system [7]. Its role is to identify clear-sky pixels in which accurate SST retrievals can be made. The ACSM is often colloquially referred to as the ‘cloud mask’, because the vast majority of the masked pixels occur due to obstruction by clouds. However, pixels can also be masked for other reasons, such as sensor issues, aerosol contamination, or atmospheric conditions that are not represented in the SST algorithm training set. The ACSM is documented in [7] with recent additions described in [1], such as reduced over-screening of dynamic SST regions and the removal of redundant filters based on the simulated BTs. In all ACSPO L2P files from LEO satellites, the SST is reported for all ocean/water pixels (all-sky domain), while  $0.02^\circ$  Level 3 files only contain clear-sky data to reduce the file size. To apply the ACSM, the user should only select pixels with  $QL = 5$  (stored in the ‘quality\_level’ variable). Additional information about land/ice coverage and day/night designation for each pixel is included in the ‘l2p\_flags’ variable. Figure 3 shows an example of Aqua MODIS nighttime ‘subskin’ SST imagery with and without the ACSM applied. Also shown is information about thermal fronts included in the ‘sst\_front\_position’ (binary indicator of the thermal SST front position) and ‘sst\_gradient\_magnitude’ (in units of K/km) variables.

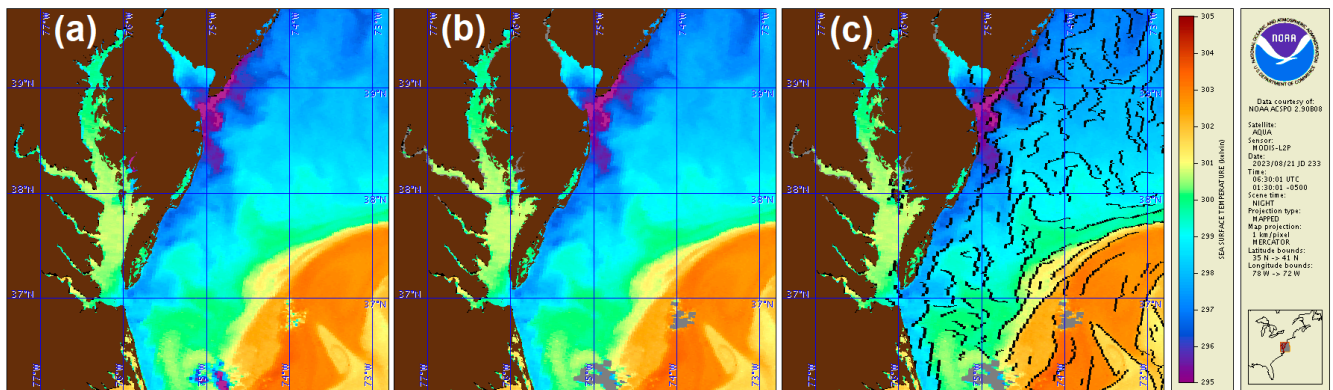


**Figure 3.** Aqua MODIS night ‘subskin’ SST imagery over Chesapeake Bay on 21 August 2023. (a) All sky SST imagery with no overlay. Land is rendered in brown. (b) ACSM mask applied (gray). (c) ACSM and front indicator (black curves) overlaid. The imagery is taken from the NOAA ACSPO Regional Monitor for the SST (ARMS) online system [30].

MODIS is a multi-detector sensor with 10 detectors per band (compared to 16 for VIIRS and 24 for the planned METImage sensor). Individual calibration of each detector may result in imagery striping, if they are not accurately co-registered. Any striping artifacts in BTs are amplified by the BT difference terms in SST retrieval Equations (1) and (2), resulting in increased SST striping. In ACSPO SST products, VIIRS and MODIS BTs go through a de-striping preprocessing step [31]. Another consequence of the multi-detector design is the well-known bow-tie effect, where imagery is distorted (more so away from nadir), and pixels near the scan edge overlap. There is also a discontinuity in the imagery between neighboring pixels from different scans. Distorted imagery degrades the ACSM, which uses spatial-window-based algorithms to identify clear-sky pixels. For this reason, in ACSPO v2.50 and later versions, imagery is resampled to correct for bow-tie distortion in all MODIS and VIIRS ACSPO data [32]. The same approach will be taken for the future METImage sensor. Another motivation for bow-tie correction is the new ACSPO thermal fronts product, which requires spatially continuous SST imagery.

Although both the MODIS and VIIRS have similar multi-detector designs, the onboard processing of sensor data differs. In order to reduce the data volume and limit pixel size growth at high VZAs, VIIRS uses an aggregation scheme where three measurements are averaged near nadir (below  $31.72^\circ$ ), two at intermediary scan angles ( $31.72\text{--}44.86^\circ$ ), and no aggregation is performed at high scan angles (above  $44.86^\circ$ ) [19]. No such aggregation is performed on MODIS, whose pixel grows from nadir to scan edge much greater (1–5 km in the across-track and 1–2 km in the along-track directions) than on VIIRS (0.75 to 1.6 km for both along and across track directions) [19,33]. Another difference in post-processing is ‘bow-tie removal’, where overlapping VIIRS pixels at scan angles above  $31.72^\circ$  are replaced with fill values to further reduce the data volume. In contrast, overlapping MODIS pixels are included in L1b data. Note that the detailed handling of bow-tie distortion and onboard deletion is only relevant for users of ACSPO L2P data and does not affect derived ACSPO L3 data, except indirectly via the improved ACSM, which may be propagated from L2P data.

#### 4. Validation of the ACSPO MODIS RAN1 SST

This section presents the validation results for the Terra and Aqua ‘subskin’ and ‘depth’ L2P SSTs against quality-controlled in situ SSTs from the NOAA iQuam v2.10 online system [15]. Note that this section analyzes the final ACSPO MODIS RAN1 dataset, produced from debiased BTs, where discontinuities and gradual drifts in the MODIS TEBs have been mitigated, as described in Section 5 and Appendix B. Note also that the performance of L3U and L3C data is comparable to that of L2P and is not analyzed here.

The included sources of in situ data are drifting and tropical moored buoys (DTMs), as well as Argo floats (AFs; presented in Appendix A). Due to the sparse geographical coverage by drifting buoys near the equator, they are often grouped together with tropical

moorings. Validation against the DTMs is presented in Section 4.1. For an intercomparison of satellite and in situ SST data in SQUAM [34], all satellite pixels within a space/time interval of [10 km × 30 min] of an in situ SST measurement are used. This results in ‘one-to-many’ matchup datasets (MDSs) where each in situ SST measurement is matched up with multiple satellite pixels. The exact number of satellite pixels matched up with a given in situ measurement depends on the size of the satellite pixel (for MODIS, 1–5 km depending on VZA) and the local clear-sky fraction near the in situ SST measurement. Only in situ SSTs with the highest iQuam quality level (QL = 5) are used.

The two main SST validation metrics are the accuracy (global mean bias with respect to DTMs) and precision (corresponding standard deviation). No formal set of NOAA SST requirements/specs exists for MODIS. In this work, we adopt the NOAA JPSS VIIRS requirements of ±0.2 K for accuracy and 0.6 K for precision [35]. A recent addition to the JPSS SST specs is that accuracy and precision requirements must be met in a clear-sky domain covering at least 18% of the global ocean or more. This additional requirement is motivated by the fact that the specs are easier met with an overly conservative clear-sky mask in a reduced clear-sky domain. Section 4.1 shows that specs are exceeded by a wide margin for both ‘subskin’ and ‘depth’ SSTs. Appendix A shows that when compared to fully independent AFs, the requirements are also met, with the exception of the Aqua daytime ‘subskin’ SST. The reason is that the AF SSTs are measured deeper (~5 m) compared to DTMs (~0.2–1.0 m), causing larger and a more variable diurnal thermocline present at the 1:30 p.m. Aqua daytime overpass time.

Table 2 lists the Aqua and Terra mean clear-sky ratios (CSRs) for both daytime and nighttime SSTs for one full year (2019) of data. Note that the CSRs do not significantly vary from year-to-year, so one-year statistics are representative for whole missions.

**Table 2.** Mean clear-sky ratios (CSRs) for ACSPO v2.80 SSTs from Aqua/Terra MODIS and NPP/N20 VIIRS. Results are from the SQUAM online system [34] using one year of data (2019).

Satellite and Sensor	CSR% Night	CSR% Day
Aqua MODIS	19.1	20.4
Terra MODIS	20.6	19.3
NPP VIIRS	18.8	19.8
N20 VIIRS	18.8	20.0

NPP and N20 VIIRS CSRs are also included, to place the MODIS RAN1 data in perspective. The 18% CSR requirement is met for all satellites, with CSRs ranging from 18.8% (NPP night) to 20.6% (Terra night). Keep in mind that cloud coverage has a diurnal cycle, possibly leading to different CSRs from Aqua (1:30 a.m./p.m.) and Terra (10:30 a.m./p.m.), whereas the NPP and N20 have similar LEXTs to Aqua [1]. Aqua CSRs are slightly higher than the NPP/N20 both at night (19.1 vs. 18.8%) and during the day (20.4 vs. 19.9%), likely due to a narrower MODIS VZA range and a larger fraction of near-nadir pixels. In addition, the Aqua retrieval sensitivity is somewhat lower compared to VIIRS, as discussed in Section 3 (0.93 vs. 0.96 in the day and 0.97 vs. 0.99 during the night). A higher SST retrieval sensitivity typically results in a lower CSR, due to reliance of the current ACSM adopted in ACSPO v2.80, on the delta between the satellite and first-guess SST [7].

Another important validation metric is the long-term stability of satellite SSTs characterized as the temporal drift in accuracy over a satellite’s mission (typically due to the TEB calibration drift). No formal NOAA requirements exist for stability, so we adopt the (A)ATSR Reprocessing for Climate (ARC) project target stability of 5 mK/year (0.05 K/decade) [36]. Section 4.2 analyzes the time series of MODIS SSTs against DTMs and shows that both Terra and Aqua SSTs meet and exceed the target stability by a wide margin.

#### 4.1. Validation of MODIS RAN1 SST against Drifting and Tropical Moored Buoys (DTMs)

Figure 4a shows the time series of the monthly number of MODIS RAN1 matchups with DTMs. To demonstrate the relative contributions of drifters and tropical moorings

(TMs) to the global validation statistics, Figure 4b shows a similar plot but for the TMs only. More than  $10^5$  monthly DTM matchups are available for the entire MODIS mission, at all times, but the relative contribution to NOBS from TMs vs. drifters has varied considerably over time. In 2000, the majority of the matchups were from the TMs. For example, in June 2000,  $0.91 \times 10^5$  out of  $1.44 \times 10^5$  Terra matchups were from TMs, or about 63%. Since 2000, the number of drifters has increased considerably, and newer drifters report SST measurements more frequently (hourly or more often), resulting in an increased number of matchups. On the other hand, the number of TMs reporting SSTs has declined since 2011, with a 75% drop in TM matchups from 2000 to the present time. In recent years, validation statistics have been dominated by drifters. For example, in June 2022, only  $2 \times 10^4$  out of  $1.4 \times 10^6$  total DTM matchups come from TMs, only about 1.4%.

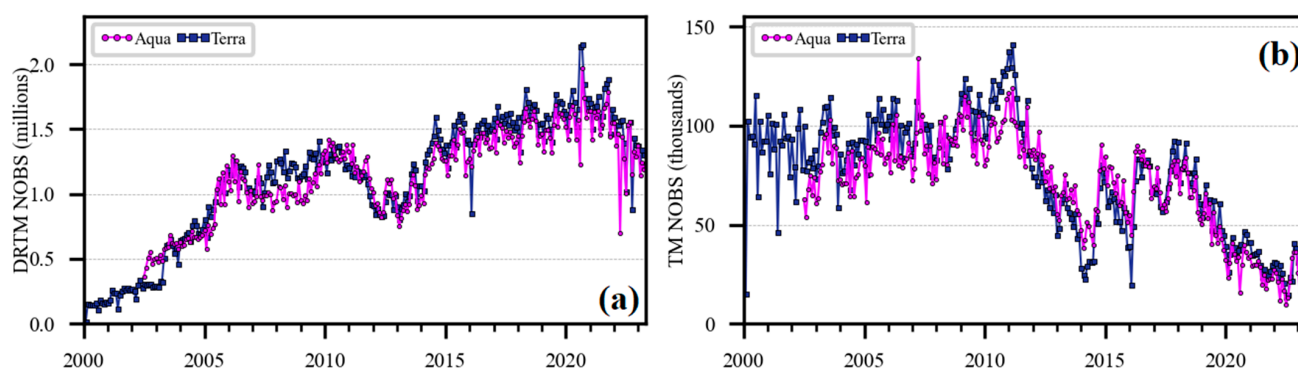
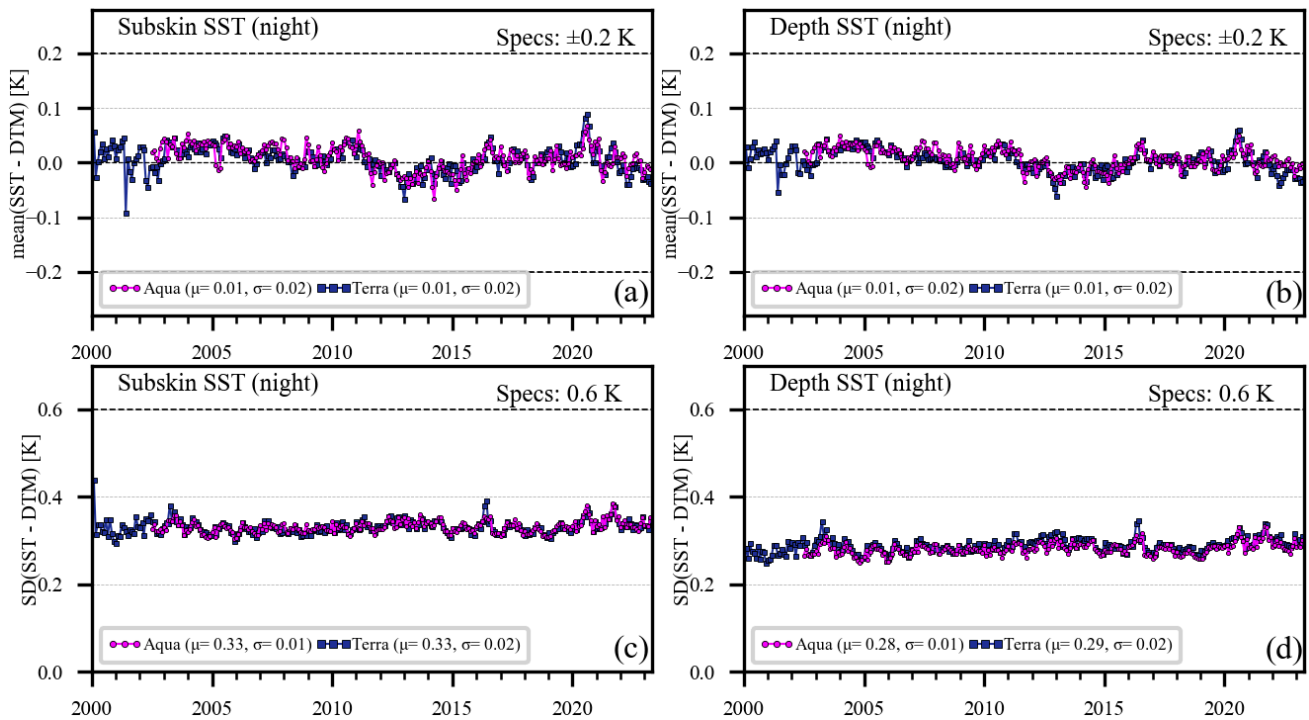


**Figure 4.** Time series of the monthly aggregated number of MODIS RAN1 nighttime matchups against (a) DTMs and (b) TMs only. Data are from the NOAA SQUAM online system [34].

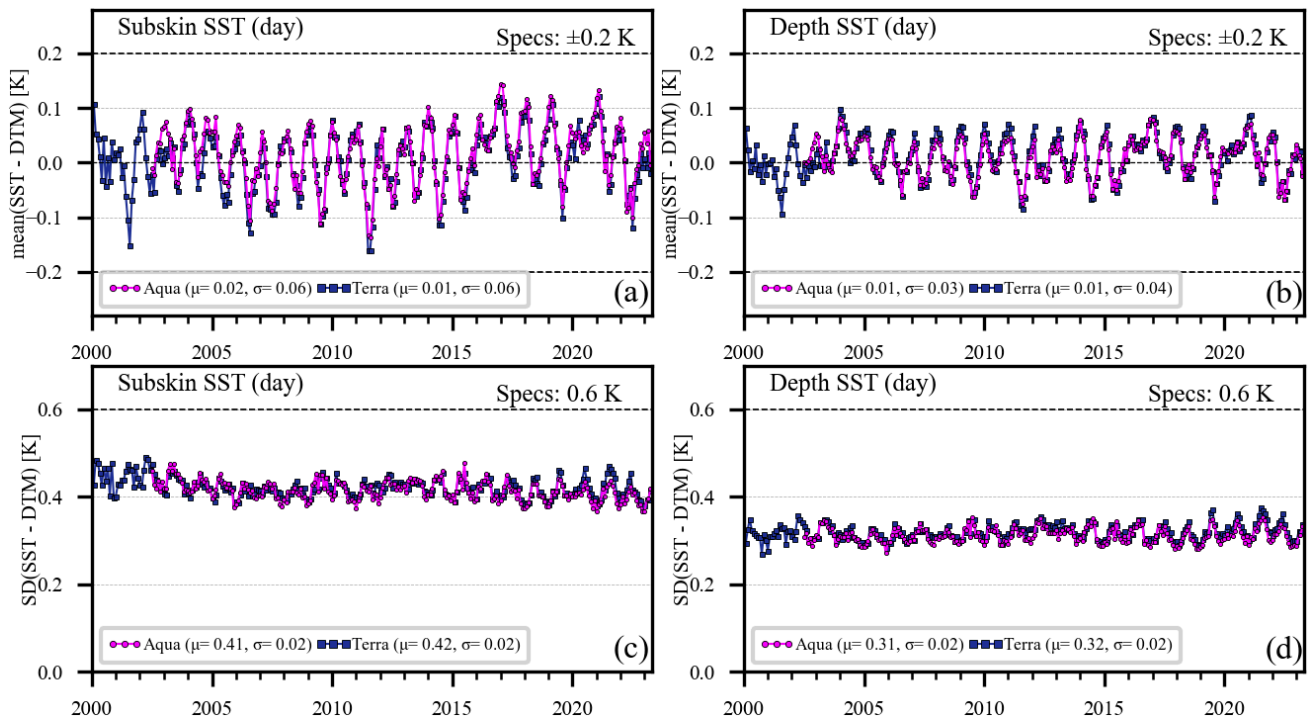
Figure 5 shows the monthly aggregated time series of the accuracy (global mean bias) and precision (corresponding standard deviation) of the MODIS nighttime ‘subskin’ and ‘depth’ SSTs against the DTMs. The NOAA specs for accuracy ( $\pm 0.2$  K) are met and exceeded for both Aqua and Terra. Typically, the accuracy is within a  $\pm 0.1$  K corridor and is often within  $\pm 0.05$  K. The precision requirement of 0.6 K is also met and exceeded, by a wide margin. As expected, the precision of the ‘depth’ SST (0.28–0.29 K) is improved compared to that of the ‘subskin’ SST (0.33 K). The Aqua and Terra accuracies and precisions agree very closely, with no visible systematic temporal change in the time series.

Figure 6 shows the corresponding daytime SST validation statistics against DTMs.

The requirements for accuracy and precision continue to be met for the daytime SST, albeit with a narrower margin. Seasonal variations in accuracy are now seen, with an amplitude of  $\sim \pm 0.1$  K for ‘subskin’ and  $\sim \pm 0.07$  K for ‘depth’ SSTs. In [1], such seasonal variations in the VIIRS accuracy were attributed to the space/time temperature difference between the skin SST and temperature at  $\sim 0.2$ – $1.0$  m measured by DTMs. If this hypothesis were correct, then such seasonal variations would be expected to be larger for Aqua and smaller for Terra, which have very different LEXTs (1:30 p.m. vs. 10:30 a.m.). However, the two curves sit on top of each other. To further rule out the skin-depth thermocline as the underlying reason, we performed an experiment where the Aqua MODIS nighttime SST record was reprocessed using the daytime SST algorithm given by Equation (2). The same seasonal bias was observed as during the daytime, suggesting that a different physical mechanism may contribute, e.g., some seasonality in the in situ DTM data or atmospheric water vapor and temperature profiles, which affects the daytime split-window NLSST more than at night with the transparent  $3.7 \mu\text{m}$  band. At the time of writing, we are unable to identify a direct link between the seasonal daytime SST biases and the atmospheric water vapor. More analyses are needed to explain this seasonality. The answer to this question is important. If there are limitations to the atmospheric correction with the split-window NLSST algorithm, then it should be revisited.



**Figure 5.** Time series of the monthly aggregated nighttime MODIS RAN1–DTM SSTs: (a,b) global mean biases (accuracy); (c,d) corresponding standard deviations (SDs; precision); (a,c) ‘subskin’ and (b,d) ‘depth’ SSTs. The corresponding temporal mean and standard deviation values for each time series are given by  $\mu$  and  $\sigma$ , respectively. Data are taken from the NOAA SQUAM online system [34].



**Figure 6.** (a–d) The same as Figure 5, but for the daytime SST.

Turning to the precision, the daytime ‘subskin’ standard deviations of  $\sim 0.41$ – $0.42$  K are degraded from their nighttime counterparts,  $\sim 0.33$  K, as expected. This is likely due to a combination of the degraded performance of the daytime split-window NLSST, due to the lack of the transparent MWIR band 20 centered at  $3.7 \mu\text{m}$ , and the increased and

more variable diurnal stratification of the upper ocean during the daytime. Consistent with the nighttime validation, daytime ‘depth’ SSTs show improved precision (0.31–0.32 K), compared to ‘subskin’ SSTs (0.41–0.42 K). More pronounced seasonality is seen in daytime standard deviations compared to their nighttime counterparts in Figure 5.

Table 3 summarizes the MODIS RAN1 validation statistics against DTMs for one full year of data (2019). Figures 5 and 6 suggest that the accuracy and precision have been stable over time, thus adding confidence that one year is representative of the full Aqua and Terra missions. The year 2019 was chosen, because the Aqua and Terra orbits remained stable, and two ACSPO VIIRS SSTs (from NPP and N20 RAN3) were available for comparison. The year 2019 was also the least affected by the anomalies in drifter data (note the ~0.05 K warm drifter SST bias from 2012–2016 manifested as a negative plateau in the MODIS time series in Figure 5a,b).

**Table 3.** MODIS validation against DTMs for the ACSPO RAN1 and NASA R2019 L2P SSTs for the year 2019 [10,11]. Results are provided with and without the SSES bias correction applied (termed ‘depth’ and ‘subskin’ SSTs in ACSPO, respectively). For comparison, validation metrics for the ACSPO NPP and N20 VIIRS RAN3 SST are also shown [1]. The validation metrics are the global mean/median biases (accuracy), conventional/robust standard deviations (SD/RSD; precision), number of observations/matchups (NOBS), clear-sky ratio (CSR), and total number of satellite pixels/observations. All metrics are presented in kelvin, except for the NOBS (unitless), CSR (%), and pixels (unitless). To facilitate a comparison between the ACSPO ‘subskin’ and NASA ‘skin’ SSTs, +0.17 K was added to NASA ‘skin’ SSTs. The same +0.17 K adjustment was applied to the NASA SSTs with the SSES bias correction (P. Minnett and K. Kilpatrick, 2023, personal communication). For the NASA R2019 products, all QL = 4 and 5 pixels were included. The nighttime NASA SST4 is produced using MWIR bands 22 and 23 [8]. The same convention for daytime (solar zenith angle  $\leq 90^\circ$ ) and nighttime ( $>90^\circ$ ) was consistently used for the ACSPO and NASA SSTs. For ACSPO, all pixels designated as clear by the ACSM were included (QL = 5). Note that due to the differences in regional coverage between DTMs and satellite data, the NOBS and CSR may not be proportional.

	SST Product	Mean Subskin	Mean Depth	Median Subskin	Median Depth	SD Subskin	SD Depth	RSD Subskin	RSD Depth	NOBS $\times 10^3$	CSR %	Pixels $\times 10^9$
Night	ACSPO Terra	+0.01	+0.00	+0.03	+0.02	0.33	0.29	0.26	0.21	19.1	20.6	16.5
	ACSPO Aqua	+0.00	+0.00	+0.03	+0.01	0.33	0.28	0.26	0.21	18.1	19.1	15.3
	ACSPO NPP	−0.01	−0.02	+0.01	−0.01	0.32	0.27	0.24	0.21	57.2	18.8	47.9
	ACSPO N20	+0.00	−0.02	+0.02	+0.00	0.32	0.28	0.24	0.22	57.4	18.8	47.9
	NASA Terra	−0.04	+0.02	+0.02	+0.06	0.40	0.40	0.28	0.28	16.3	17.7	14.2
	NASA Aqua	−0.13	−0.04	−0.06	0.00	0.40	0.41	0.28	0.29	15.5	16.3	13.1
Day	ACSPO Terra	+0.02	+0.01	+0.03	+0.02	0.42	0.33	0.37	0.27	17.6	19.3	15.7
	ACSPO Aqua	+0.03	+0.01	+0.04	+0.02	0.42	0.31	0.35	0.26	16.9	20.4	16.6
	ACSPO NPP	−0.03	+0.00	−0.02	+0.01	0.38	0.28	0.29	0.22	53.2	19.8	51.2
	ACSPO N20	−0.04	+0.00	−0.03	+0.01	0.38	0.29	0.30	0.23	53.6	20.0	51.4
	NASA Terra	−0.02	−0.02	+0.01	+0.00	0.50	0.50	0.43	0.43	21.2	22.6	18.4
	NASA Aqua	−0.03	−0.03	+0.00	+0.00	0.47	0.47	0.39	0.39	19.5	22.6	18.5

To put the MODIS RAN1 in the context of other available similar products, Table 3 lists the performance statistics for the VIIRS RAN3 [1] and NASA R2019 MODIS data [10,11]. For the R2019, all pixels with QLs = 4 and 5 are included. This criterion results in a comparable fraction of clear-sky pixels between the ACSPO and NASA products. Excluding QL = 4 pixels improves the NASA validation metrics, but results in a significantly reduced clear-sky domain (by >30%; e.g., all pixels with VZA  $> 55^\circ$  are flagged as QL = 4 in the NASA product, in contrast to ACSPO, where QL = 5 retrievals are made in a full sensor swath). Note also that the NASA product reports ‘skin’ SSTs (calculated by subtracting 0.17 K from the regressions trained against DTMs, P. Minnett, K. Kilpatrick, 2023, personal communication). For consistency with the ACSPO ‘subskin’ SSTs, +0.17 K was added to all NASA SSTs.

The RAN1 ‘subskin’ and ‘depth’ SSTs accuracies and precisions are largely consistent between Terra and Aqua. The precision of the ACSPO ‘depth’ SST is improved over the ‘subskin’ (by  $\sim 0.05$  K at night and by  $\sim 0.10$  K during the day). The corresponding standard deviations are inferior compared to VIIRS (by  $\sim 0.02$  K at night and  $\sim 0.05$  K during the day), presumably due to the use of the M14 band centered at  $8.6 \mu\text{m}$  in the VIIRS retrievals. This band has a lower impact at night, due to a dominant contribution from the MWIR  $3.7 \mu\text{m}$  band. The CSRs are largely consistent across all ACSPO VIIRS and MODIS products. (Recall that the CSR is defined as the ratio of the SST pixels to all ice-free ocean pixels measured by the sensor and serves as a measure of the efficiency of the clear-sky mask). The global coverage (actual area covered by SSTs) is significantly greater for VIIRS compared to MODIS, due to the considerably wider swath ( $3060 \text{ km}$  vs.  $2330 \text{ km}$ ). The wider swath and higher resolution of VIIRS results in about  $\times 3$  more satellite pixels, compared to MODIS.

The RAN1 performance is improved over that of R2019. At night, the ACSPO ‘subskin’ standard deviations are  $\sim 0.33$  K vs.  $\sim 0.40$  K for NASA. The RSD margin of improvement is narrower,  $0.26$  K vs.  $0.28$  K. The corresponding daytime metrics are  $0.42$  vs.  $0.47\text{--}0.50$  K for the conventional standard deviation, and  $0.35\text{--}0.37$  vs.  $0.39\text{--}0.43$  K for the RSD.

Subtracting the SSES bias (equivalent to obtaining ‘depth’ SST in ACSPO) statistically significantly improves the ACSPO standard deviations and RSDs but has little effect on the NASA statistics, in part due to the not very effective choice of scale factor ( $0.16$  K) in the ‘sses\_bias’ field in the NASA files. Recall that as per the GDS2 standards, this variable is stored as a signed eight-bit integer with an associated offset and scale factor. The scale factor determines the quantization of the ‘sses\_bias’ variable, and  $0.16$  K is too large. In the ACSPO files, the SSES bias scale factor is  $0.016$  K. Because of the differences in the SSES algorithms and numerical implementations, the margin in the performance metrics between the ACSPO ‘depth’ SSTs and the SSES-bias-corrected NASA SSTs is wider compared with the ‘subskin’ SST.

At night, the ACSPO NOBSs (number of matchups with DTMs) are larger than NASA NOBSs:  $20.6$  M (Million) vs.  $17.7$  M for Terra and  $19.1$  M vs.  $16.3$  M for Aqua. During the daytime, ACSPO has fewer matchups:  $19.3$  M vs.  $22.6$  M for Terra and  $20.4$  M vs.  $22.6$  M for Aqua. Adding up the night and day NOBSs, one obtains the following ACSPO vs. NASA statistics:  $39.9$  M vs.  $40.3$  M for Terra, and  $39.5$  vs.  $39.9$  M for Aqua, which are within 1% of each other. ACSPO day/night NOBSs are more closely balanced than NASA, which may be due to different definitions of day and night in ACSPO and NASA processing.

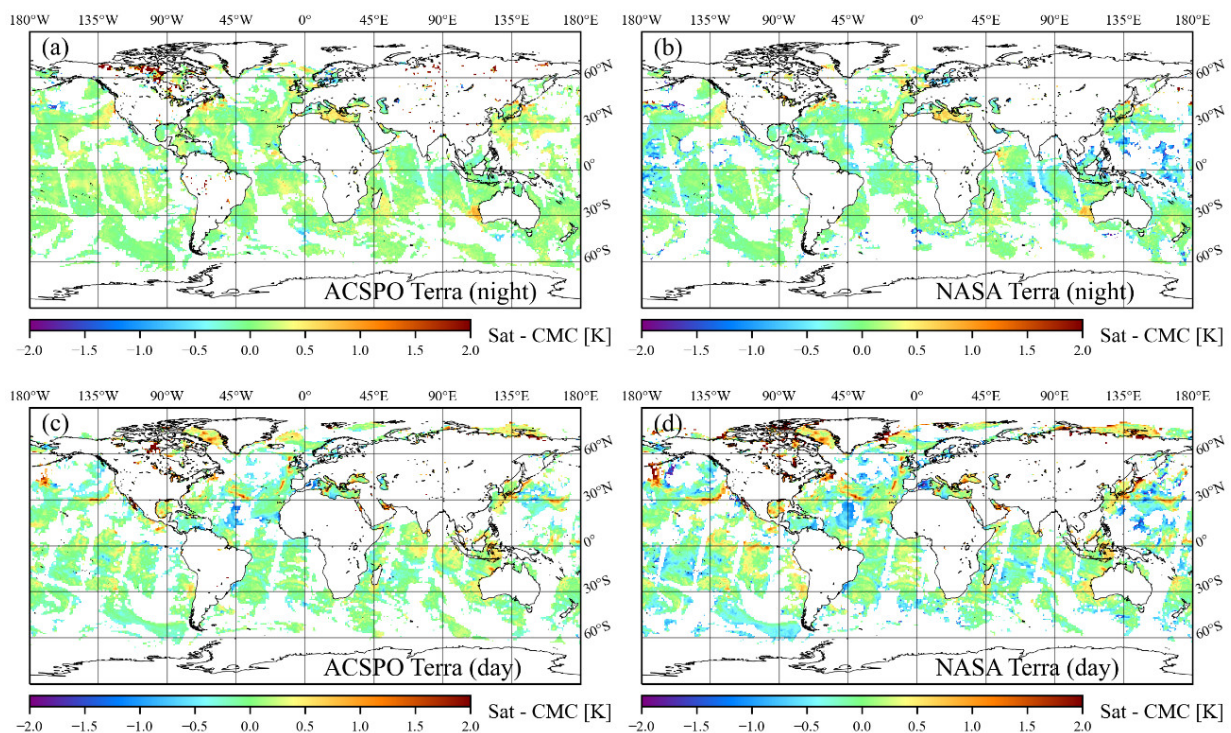
Additional analyses in Appendix A provide validation against Argo Floats (AFs). These are largely consistent with the DTM analyses above but being fully independent, provide an additional important consistency check.

ACSPO CSRs are larger than NASA CSRs at night ( $20.6\%$  vs.  $17.7\%$  for Terra and  $19.1\%$  vs.  $16.3\%$  for Aqua), and smaller during the daytime ( $19.3\%$  vs.  $22.6\%$  for Terra and  $20.4\%$  vs.  $22.6\%$  for Aqua). The ACSPO mask thus appears more liberal than NASA at night and more stringent during the daytime.

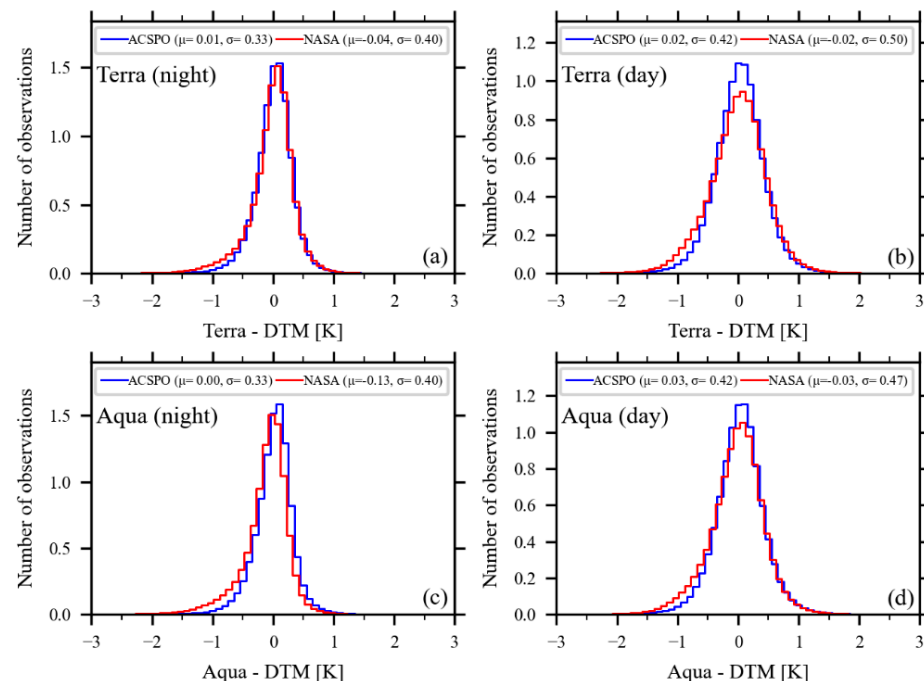
Figure 7 shows 24 h aggregated global maps of the Terra ACSPO and NASA SST biases against the gap-free Canadian Meteorological Centre (CMC) L4 foundation SST [37] for both night and day, for one representative day of data, 1 August 2019. Bluish spots, seen in both products, suggest residual cloud or aerosol leakages. Those are more frequent and pronounced in the NASA SST. Terra was chosen for this demonstration because of the suppressed diurnal signal and, hence, the expected closer proximity of satellite SST to the CMC L4 foundation SST. The Aqua patterns are similar. Apart from residual cloud leakage, the agreement between the ACSPO and NASA SSTs is quite close, with no systematic regional differences visible in Figure 7. Both the ACSPO and NASA daytime SSTs exhibit cold biases in the North Atlantic between  $10^\circ\text{N}$  and  $30^\circ\text{N}$ , likely due to dust aerosols originating from the Sahara Desert in Northern Africa.

Figure 8 compares ACSPO and NASA histograms of bias with respect to DTMs for the one-year period analyzed in Table 3. The NASA histograms are less symmetric and show a more pronounced cold tail. This is consistent with the higher NASA standard deviations

and RSDs shown in Table 3 (and a wider margin between those), and the increased residual cloud leakage seen in Figure 7.



**Figure 7.** Twenty-four-hour aggregated mean biases of the Terra MODIS—CMC L4 foundation SST [37]. SST data are from 1 August 2019: (a,c) RAN1 ‘subskin’; (b,d) R2019 ‘skin’; (a,b) night; (c,d) day. A +0.17 K offset was added to the NASA ‘skin’ SST to facilitate its comparison with the ACSP0 ‘subskin’ SST.



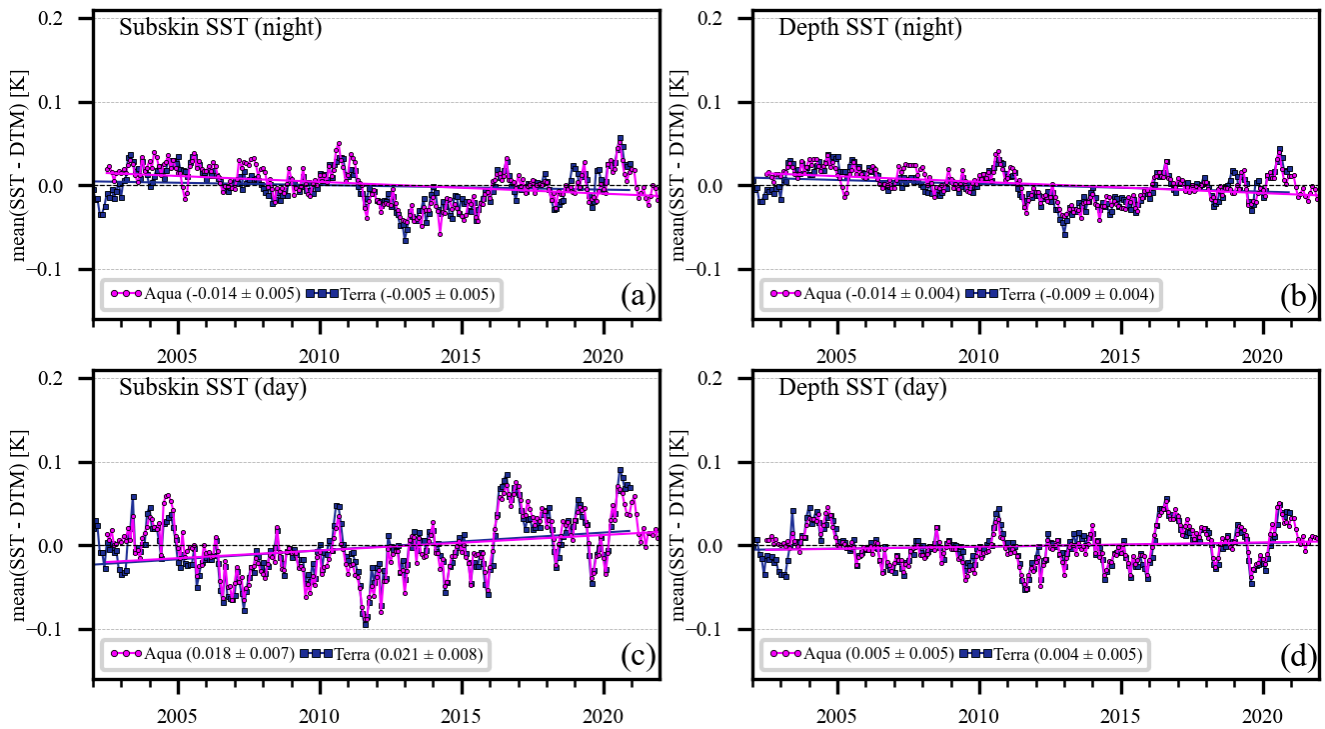
**Figure 8.** Yearly (2019) aggregated histograms (binned at 0.1 K) of MODIS—DTM ‘subskin’ SSTs: (a,b) Terra; (c,d) Aqua; (a,c) night; (b,d) day. Each panel shows (blue) ACSP0 ‘subskin’ SST and (red) NASA ‘skin’ SST + 0.17 K. The histograms are normalized with the total area under each curve = 1. For each histogram, the mean ( $\mu$ ) and standard deviation ( $\sigma$ ) in Kelvin are listed in the legend.

#### 4.2. Long-Term Stability

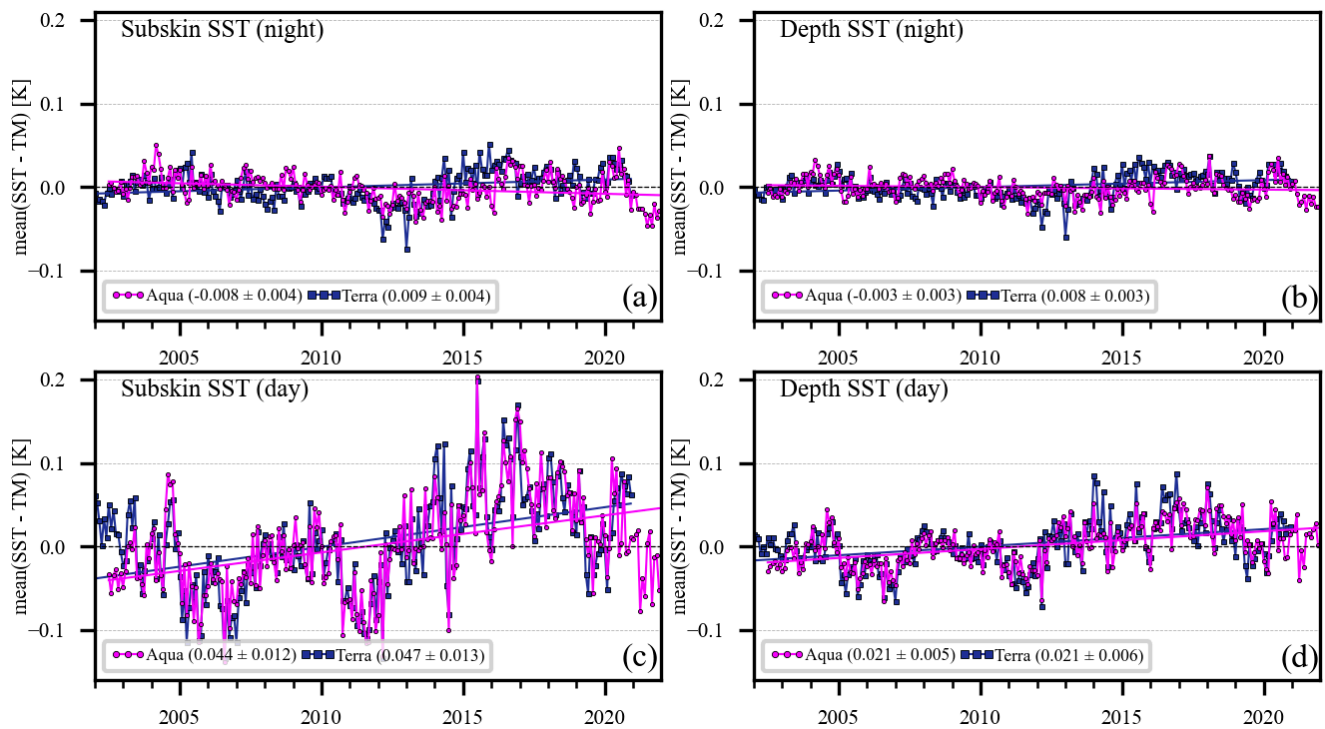
Estimating the stability of the satellite SST via a comparison with the in situ SST is a nontrivial task due to uncertainties inherent in the in situ data themselves. Both drifters and TMs have their pros and cons when it comes to stability estimation. It may not be easy to separate drift in satellite SSTs from regional biases modulated by changes in the drifter geographical distribution. An improved accuracy, stable geographical distribution, and reduced seasonality near the equator make TMs attractive for studying the long-term stability of satellite SSTs, as has been explored in the (A)ATSR Reprocessing for Climate (ARC) and JPSS VIIRS RAN3 [1,36]. However, TMs are less numerous than drifters, leading to noisier validation statistics. The deeper TM measurements (~1 m) also pose a challenge for validation during the daytime, when a significant diurnal thermocline may be present. Another challenge with using TMs is the lack of atmospherically transparent MWIR bands during the daytime, making satellite SST retrieval through the humid tropical atmosphere less accurate. For the reasons listed above, we present analyses of the long-term stability of the MODIS RAN1 SST using both DTMs and TMs as references. We omit AFs from the stability analysis for two reasons: (1) there were very few AF platforms in the early 2000s, and their fleet was rapidly changing; and (2) the depth of their shallowest SST measurements evolved over time. Since 2013, some AFs have started to report near-surface SSTs as shallow as 0.2 m, compared to the typical ~5 m depth reported in the 2000s [38]. The challenge of the varying AF measurement depth can be overcome by using the SST measurement nearest to 5 m from a given AF profile. However, the current iQuam v2.10 designed in 2008 selects the shallowest high-quality SST from a given profile. The NOAA SST team is exploring the inclusion of the measurement closest to a chosen nominal depth of ~5 m, in addition to keeping the shallowest AF measurement.

Figure 9 shows the time series of the  $\Delta T_S = \text{MODIS RAN1} - \text{DTM SST}$  mean bias for both 'subskin' and 'depth' SSTs during the day and night. Linear trends obtained using least square fits are also overlaid. Note that Figure 9 and all further stability estimates in this section only employ time periods with stable LEXTs (1 January 2002–31 December 2020 for Terra and 4 July 2002–31 December 2021 for Aqua) to minimize the effect of the variable local observation time. Figure 9a,b shows that the drift is  $\sim -0.014$  K/decade for Aqua (for both 'subskin' and 'depth'  $\Delta T_S$ s) and  $\sim -0.005$  and  $-0.009$  K/decade for Terra 'subskin' and 'depth' SSTs, respectively. We attribute (at least partially) the slightly negative drifts in the nighttime  $\Delta T_S$ s, consistent between Aqua and Terra, to a systematic  $\sim 0.05$  K warm bias in iQuam drifter data between 2012 and 2016 (also observed in ACSPO VIIRS SST [1]). Figure 9c,d shows the corresponding daytime  $\Delta T_S$ . For Aqua, the drifts are  $+0.018$  and  $+0.005$  K/decade for the 'subskin' and 'depth' SSTs, respectively. For Terra, they are  $+0.021$  and  $+0.004$  K/decade for the 'subskin' and 'depth' SSTs, respectively.

Figure 10 shows the same stability analysis as in Figure 9 but uses TMs as a reference. Figure 10a,b shows that both Terra and Aqua nighttime  $\Delta T_S$ s have remained very stable when compared to the TMs, with estimated drift magnitudes of below 0.01 K/decade for both the 'subskin' and 'depth' SSTs. The small nighttime SST trends vs. TMs are counter-directed for Aqua (negative) and Terra (positive), in contrast to the trends against the DTMs (Figure 9a,b) which are all negative. Figure 10c,d shows the daytime results. While still meeting the target stability of 0.05 K/decade, the estimated daytime drifts vs. TMs are all positive and are considerably larger compared to the nighttime counterparts ( $\sim +0.045$  vs.  $\sim \pm 0.01$  K/decade for 'subskin' and  $0.021$  vs.  $\sim 0$  K/decade for 'depth'). The estimated daytime drifts against TMs are significantly larger than those against DTMs (Figure 9c,d), possibly due to the stronger diurnal thermocline at TM SST depths (~1 m) and the absence of atmospherically transparent MWIR channels in the daytime satellite SST algorithm. Furthermore, the TM daytime results after 2011 show increased noise, likely due to the significantly decreased number of TM matchups after 2011 (cf. Figure 4b).



**Figure 9.** Time series of the monthly aggregated nighttime  $\Delta T_S = \text{MODIS RAN1} - \text{DTM}$  SST mean biases: (a,b) night; (c,d) day; (a,c) ‘subskin’; (b,d) ‘depth’ SSTs. The seasonal signal was subtracted using the STL (Seasonal and Trend decomposition using Loess) algorithm [39]. The figure legends list the slopes and associated uncertainties (in units of K/decade) obtained using a linear least square fit with a 95% confidence interval. The lines correspond to linear fits.



**Figure 10.** (a–d) Same as in Figure 9, except against TMs instead of DTMs.

Estimates of the ACSPO MODIS RAN1 daytime and nighttime  $\Delta T_S$  trends are summarized in Table 4 against both DTMs (from Figure 9) and TMs (from Figure 10).

**Table 4.** Drifts in the ACSPO MODIS RAN1 global mean biases (K/decade) and associated uncertainties corresponding to a 95% confidence interval. Results are shown vs. both DTMs and TMs.

Ref.	SST	Terra	Aqua
DTM	Night 'subskin'	$-0.005 \pm 0.005$	$-0.014 \pm 0.005$
	Night 'depth'	$-0.009 \pm 0.004$	$-0.014 \pm 0.004$
	Day 'subskin'	$+0.021 \pm 0.008$	$+0.018 \pm 0.007$
	Day 'depth'	$+0.004 \pm 0.005$	$+0.005 \pm 0.005$
TM	Night 'subskin'	$+0.009 \pm 0.004$	$-0.008 \pm 0.004$
	Night 'depth'	$+0.008 \pm 0.003$	$-0.003 \pm 0.003$
	Day 'subskin'	$+0.047 \pm 0.013$	$+0.044 \pm 0.012$
	Day 'depth'	$+0.021 \pm 0.006$	$+0.021 \pm 0.005$

All  $\Delta T_S$ s meet the target stability of  $\pm 0.05$  K/decade. At night, analyses vs. TMs are deemed more reliable due to the 2012–2016 systematic cold bias against DTM SSTs, which is common to both Aqua and Terra MODISs (as well as NPP/N20 VIIRS SSTs [1]). For daytime SSTs, on the other hand, the estimates against DTMs appear to be more realistic, due to the significant noise in the  $\Delta T_S$  time series vs. TMs in Figure 10c,d. For the remainder of this paper, the reported stability estimates for night SST are based on the TMs, whereas for the day SST, they are based on the DTMs. With this choice, both day and night Aqua/Terra 'depth', as well as the night 'subskin' trends, are well within  $\pm 0.01$  K/decade. The daytime 'subskin' SST drift is largest, on an order of  $+0.02$  K/decade for both Terra and Aqua. Considerably reduced drift in the daytime 'depth' SST (computed using piecewise regression) compared to the 'subskin' SST (computed using global regression) may be due to an interplay between seasonal biases (which are reduced in the 'depth' SST) and the evolving DTM global geographical distribution.

## 5. Mitigation of MODIS Thermal Emissive Band (TEB) Calibration Anomalies

We reiterate that Section 4 validated the final MODIS RAN1 product, after the Collection 6.1 Terra and Aqua BTs had been corrected and debiased to mitigate remaining residual steps/discontinuities and drifts in brightness temperatures (BTs). These procedures are documented in this section, with additional details provided in Appendix B.

The analyses are split into three parts, dealing with three different types of calibration artifacts. Note that the MODIS Collection 6.1 addressed and mitigated many artifacts in radiances. However, residual BT instabilities, although small, are amplified by Equations (1) and (2) and should be mitigated to generate a science-quality data record.

Section 5.1 deals with the correction of discontinuities in Terra MWIR BTs, due to early mission changes in the Terra MODIS operating configuration. Section 5.2 analyzes the long-term stability of the Aqua and Terra LWIR and MWIR BTs and SSTs and describes the mitigation strategy. Mitigation of the relatively smaller Terra MODIS LWIR and MWIR calibration artifacts, due to changes in the Terra MODIS blackbody temperature (BBT), have less effect on the long-term SST stability, and are covered in Appendix B.

### 5.1. Mitigation of Early-Mission Terra BT Anomalies

Since its launch on 18 December 1999, the Terra MODIS instrument has operated in four different configurations [40,41]:

1. 'AA1': A-side electronics and A-side formatter (launch–30 October 2000)
2. 'BB': B-side electronics and B-side formatter (BB) (30 October 2000–15 June 2001)
3. 'AA2': A-side electronics and A-side formatter (2 July 2001–17 September 2002)
4. 'AB': A-side electronics and B-side formatter (17 September 2002–present)

These changes are known to affect the calibration of Terra MWIR bands and cause discontinuities in MODIS nighttime SSTs [9]. Figure 11a shows the time series of the global mean nighttime 'subskin' SST biases (with respect to the CMC L4 foundation SST) observed during our first pass through the MODIS data using the original C6.1 L1b data. Two SST steps were observed:  $\sim +0.12$  K on 30 October 2000, associated with the switch from the AA1

to the BB configuration, and  $\sim +0.14$  K on 2 July 2001. The second step followed the 17-day data gap from 15 June 2001 to 2 July 2001 due to a Terra MODIS power supply failure, which in turn, triggered the switch from the BB to the AA2 configuration. No discontinuity was found to be associated with the switch from AA2 to AB on 17 September 2002 (not shown in Figure 11).

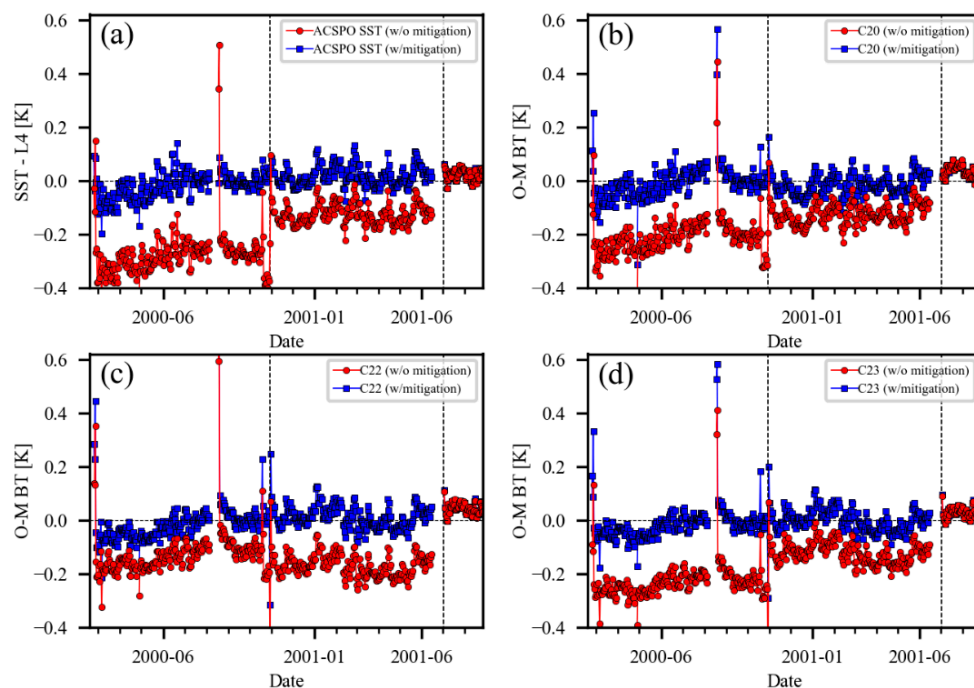


**Figure 11.** (a) Twenty-four-hour aggregated ACSP0 ‘subskin’—CMC L4 SST global mean biases; ‘O-M’ BT for bands (b) 20, (c) 22, and (d) 23 (blue circles) with and (red circles) without the mitigation of BTs. The two vertical dashed lines mark the dates when the Terra MODIS operating configuration changed from AA to BB (30 October 2000) and from BB to AA2 (2 July 2001). For easier viewing, the results are shifted vertically with the convention that time series with mitigation are centered on zero. For a further explanation, see the main text.

In [8], the authors addressed the SST discontinuities by training three separate sets of SST retrieval coefficients separately for the AA1, BB, and AA2/AB configurations. The complication here is that the AA1 and BB both lasted less than a year. The short time series, in conjunction with the relatively scarce in situ SST data from the early 2000s ( $\sim 6 \times 10^3$  daily drifting buoy observations in 2000 compared to  $(20\text{--}35) \times 10^3$  after 2006 [15]) resulted in a suboptimal number of matchups for training SST regression coefficients.

In RAN1, we opted to debias the Terra MODIS MWIR BTs to the longest stable AA2/AB period using band- and configuration-specific offsets. The constant BT offsets were determined visually from the time series in Figure 11 and listed in Table 5, along with the corresponding  $\Delta$ SSTs. Note that the ACSP0 nighttime SST algorithm only employs one MWIR band (20). Bands 22 and 23 are not used in ACSP0. However, they were used in R2019 and included in Figure 11 and Table 5, for completeness.

**Table 5.** Estimated ACSP0 SST and MWIR BT offsets in the two earlier Terra MODIS configurations, AA1 and BB, relative to the current AA2/AB configuration (using the time series in Figure 11).

Configuration	SST Bias [K]	Band 20 Bias [K]	Band 22 Bias [K]	Band 23 Bias [K]
AA1	−0.26	−0.20	−0.11	−0.21
BB	−0.14	−0.11	−0.18	−0.12

In addition to the two steps, several other instances of MWIR calibration anomalies took place in the early Terra period from 24 February–31 October 2000, which resulted in abnormally warm MWIR BTs and SSTs (identifiable as outliers in the time series in Figure 11). The affected dates are 24–26 February 2000 (the first 3 days of Terra TEB data), 18–19 August 2000 (the first 2 days following an extended outage due to a MODIS formatter anomaly [42]), 19 October 2000 (WUCD event) and 31 October 2000 (the first day after switch to the BB configuration). The warm MWIR anomalies resulted in the SST biases visible in Figure 11a with daily global means from 0.1 to 0.7 K. No LWIR BT discontinuities were observed at the time of these MWIR anomalies. To mitigate the effect of warm MWIR biases on the nighttime SST, a two-band LWIR NLSST algorithm (trained using 2016–2021 nighttime matchups) was employed for these anomalous dates. As shown in Section 4.1 and Appendix A, in the absence of the more transparent band 20, the use of the LWIR algorithm reconciles the biases but slightly increases the global standard deviations.

### 5.2. Mitigation of MODIS TEB Calibration Drifts

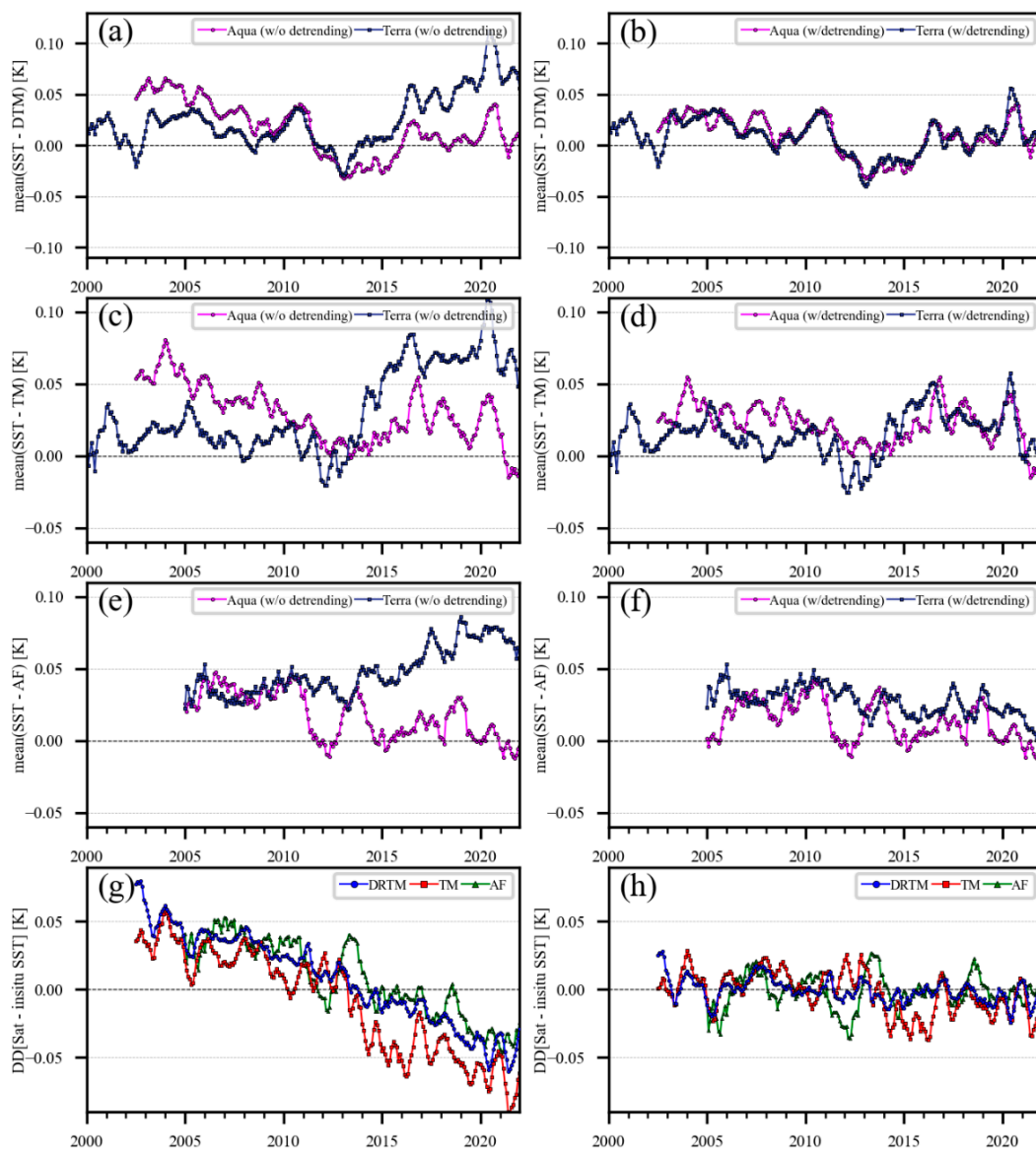
This section describes mitigation strategies for drifts in MODIS BTs over the duration of the Aqua and Terra missions. Analyzing long term trends is more challenging than dealing with step changes, because special care must be taken to distinguish the effects caused by sensor degradation from those caused by the evolution of the ‘ground truth’ data. In situ data are often considered the ‘gold standard’, but they are also subject to changes in the sensor technology, SST measurement depth, and geographical distribution, which can affect long-term trends of the satellite vs. the in situ SST bias. Modeled radiances used for observed minus modeled (‘O-M’) BT analyses may also be subject to drifts, due to potential long-term trends in CRTM inputs (CMC L4 SST and MERRA atmospheric profiles). We begin this section by analyzing a long-term time series of MODIS  $\Delta T_{SS}$ , against three widely used types of in situ SST data—DTMs, TMs, and AFs. We then compare the  $\Delta T_S$  drifts with the ‘O-M’ BTs and propose a detrending scheme to stabilize the BTs. We show that the detrending of BTs mitigates residual MODIS  $\Delta T_S$  drifts against in situ SSTs, resulting in more stable ACSPO MODIS RAN1 SSTs. To minimize the effect of the Aqua and Terra orbital drifts on the ‘O-M’ BTs, we only consider dates prior to 31 December 2021, when the orbits of both Aqua and Terra remained stable (see Figure 1).

Figure 12a–f shows the time series of the ACSPO MODIS nighttime ‘subskin’  $\Delta T_{SS}$  vs. the DTMs, TMs, and AFs.

Before detrending, the time series in the three top-left panels show evolutions of the nighttime  $\Delta T_{SS}$ , which are largely consistent across the DTMs, TMs, and AFs but different between Terra and Aqua. From the beginning of the Aqua mission in 2002, its  $\Delta T_{SS}$  gradually decreased for about a decade and then stabilized themselves after ~2012. In contrast, the Terra  $\Delta T_{SS}$  were more stable during the first decade and then increased. To estimate the Terra minus Aqua cross-sensor biases, the corresponding double differences (DD) were calculated as  $DDs = (T_{S,Aqua} - T_{S,IS}) - (T_{S,Terra} - T_{S,IS})$ , separately for IS = DTM, TM, and AF. When calculating the DDs, the  $T_{S,IS}$  (approximately) cancel out and the resulting DDs (approximately) represent  $(T_{S,Aqua} - T_{S,Terra})$ .

The three corresponding DDs are plotted in the bottom-left panel. They are highly consistent between the DTMs, TMs, and AFs, all showing near-linear trends of the order ~0.1 K over 20 years. The time series in the right panels of Figure 12 show that the use of detrended BTs successfully mitigates trends in  $\Delta T_{SS}$  and, importantly, reconciles them between Terra and Aqua. Later in this section, we describe the details of the detrending algorithm and show that the main contributor to the MODIS nighttime SST trends is drifting BTs in the MODIS MWIR band 20, which is the main contributor to the ACSPO nighttime SST (cf. Table 1).

Figure 13 shows the same results as in Figure 12, but for daytime MODIS SSTs.



**Figure 12.** (a–f) Monthly aggregated global mean biases of the  $\Delta T_S = \text{ACSPO MODIS nighttime 'subskin' } T_{SAT}$  minus the (a,b) DTM, (c,d) TM, (e,f) AF  $T_{IS}$ . (g,h) The corresponding 'Aqua minus Terra' double differences (DDs). Left panels (a,c,e,g): Results with the original MODIS BTs. Right panels (b,d,f,h): Results with the detrended MODIS BTs. To suppress noise, the DTM and TM time series were smoothed with a 7-month sliding window average, centered at current month. A 13-month window was used for the AFs, due to their two orders of magnitude fewer matchups.

Compared to Figure 12, the time series in the top three left panels in Figure 13a,c,e are less consistent across the three in situ SSTs. This may be because daytime Terra and Aqua  $\Delta T_S$  are differently affected by the SST diurnal cycle and are further modulated by different measurement depths for the various  $T_{IS}$ : drifters ( $\sim 0.2$  m), TMs ( $\sim 1$  m), and AF ( $\sim 5$  m). The Terra daytime overpass occurs at 10:30 a.m., and its SSTs are less subject to diurnal warming than Aqua at 1:30 p.m. Terra shows an upward trend in  $\Delta T_S$  vs. all three in situ SSTs. On the other hand, Aqua does not exhibit clear signs of systematic SST drift, consistently between the three in situ SSTs. Figure 13b,d,f shows that when using detrended BTs, the Terra SST agrees better with the more stable Aqua, although residual inter-annual biases of up to  $\sim 0.1$  K remain for both satellites. A noticeable trend remains for Terra SST vs. AFs, even after the BTs were detrended. This could be due to the increased fraction of near-surface AF measurements in recent years, coupled with a change in the time-of-day AFs reported for the SST (cf. Appendix A). Later in this section, we show that

the cause of the upward Terra daytime trend is drift in MODIS LWIR bands 31 and 32 used in the ACSPO daytime SST.

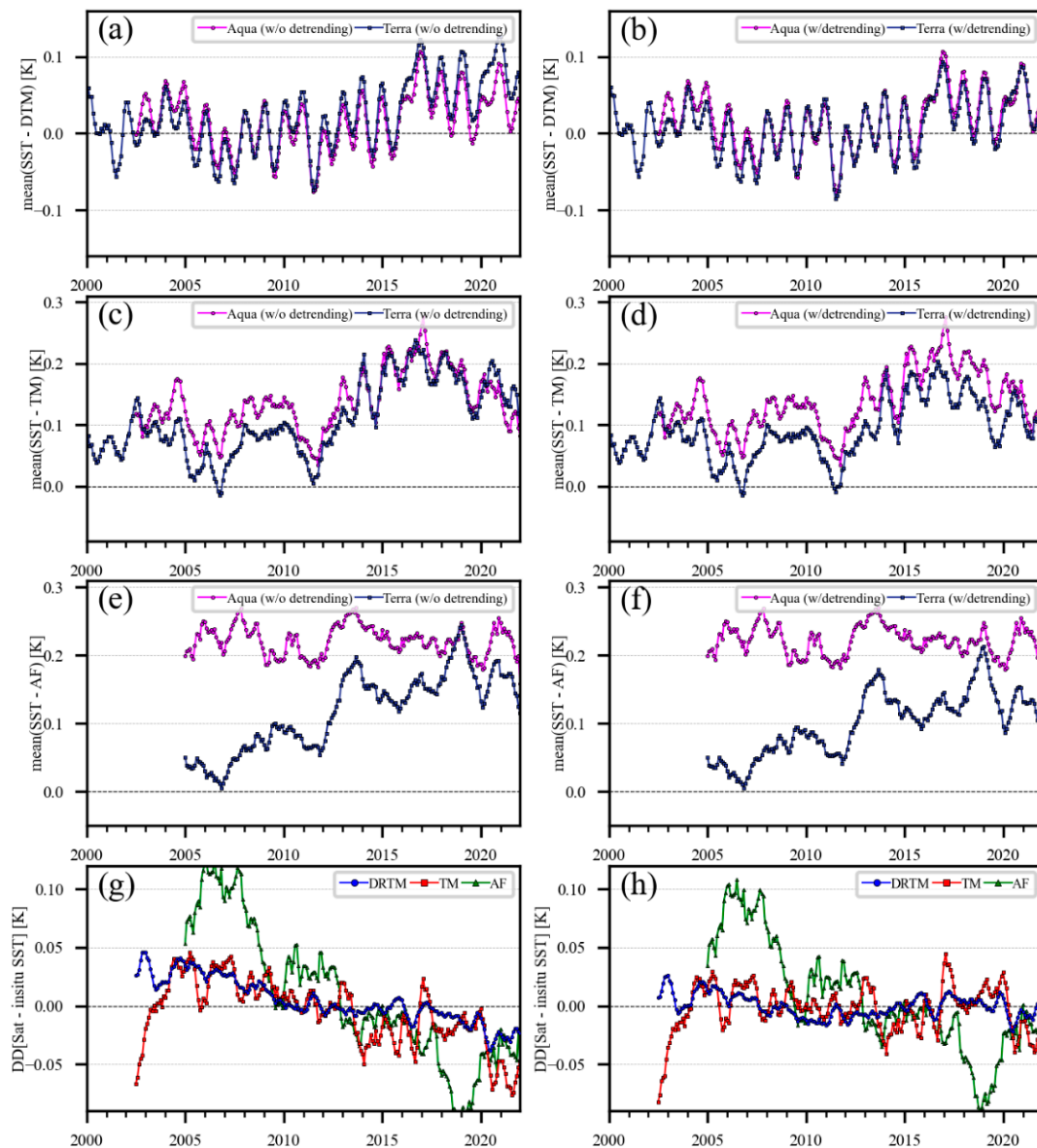


**Figure 13.** (a–h) Same as in Figure 12 but for daytime.

Below, we analyze the stability of the MODIS BTs over the course of the Aqua and Terra missions and propose a detrending scheme to correct their residual drifts. Our approach is based on the analysis of long-term trends in the observed minus modeled ('O-M') BTs. Figures 12 and 13 show that SST drifts at an order of  $\sim 0.1$  K occur over the course of the Aqua and Terra missions. The contributions of individual bands to the SST in Table 1 suggest that the associated drifts in BTs are expected to be even smaller. The small magnitude and long time frame (over 20 years) make it challenging to differentiate between the portion of the 'O-M' BT drift coming from the observed ('O') vs. the modeled BTs ('M'; recall that those are calculated using the CRTM with the first-guess CMC L4 foundation SST [37,43] and MERRA-2 atmospheric profiles [44–46] as inputs).

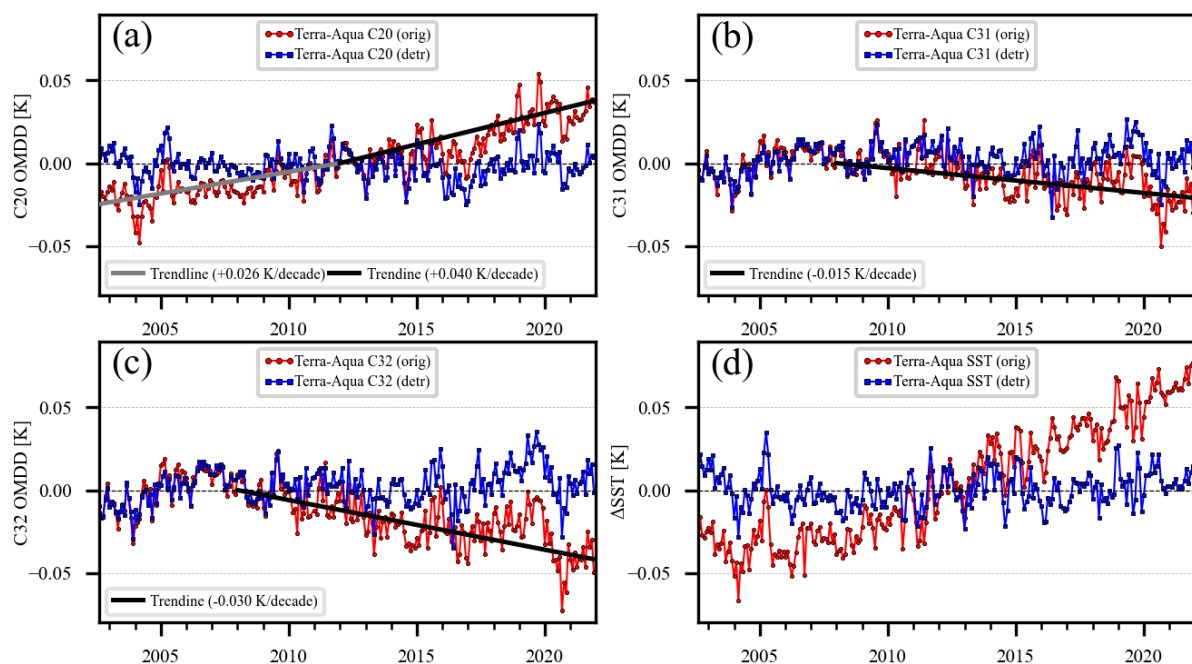
To identify contributions to the 'O-M' BT drifts from the observed BTs, we additionally analyze the Terra-Aqua 'O-M' DDs. We also compare MODIS SSTs with the NPP VIIRS and Envisat AATSR SSTs, for an additional independent consistency check.

Similar to the  $\Delta T_S$  DDs, the premise of the 'O-M' DDs is that the 'M' component of the drift cancels out, leaving only the 'O' (measured) BT component. However, 'O-M' DDs

can only characterize the consistency between two sensors and cannot tell which of the two is stable and which drifts. We address this issue by analyzing the ‘O-M’ DD trends in conjunction with data in Figures 12 and 13 which suggest, ‘by a preponderance of the evidence’, which sensor and during what periods the SST was likely stable. The hope is that, for each time interval, at least one sensor is ‘stable’ and can be used as a reference, to which the other ‘unstable’ sensor may be linked. Here, we only analyze bands 20, 31, and 32 and omit MWIR MODIS bands 22 and 23, which are currently not used in ACSPO, thus preventing linking stability of their ‘O-M’ DDs with the ACSPO SSTs.

The procedure used to calculate the ‘O-M’ DD for a pair of satellites/sensors is as follows: First, monthly aggregated mean ‘O-M’ biases are calculated for all considered bands on a global  $0.1^\circ$  equiangular grid, separately for Aqua and Terra. The Terra–Aqua ‘O-M’ DDs are then calculated by taking differences between the pairs of monthly aggregated ‘O-M’ biases and computing their global average over all  $0.1^\circ$  grid cells with at least 10 monthly observations or more. The procedure is repeated for each month, providing a monthly aggregated time series of Terra–Aqua ‘O-M’ DDs. In order to cross compare trends in ‘O-M’ BT DDs with  $\Delta T_{\text{S}}$  DDs, we also compute their global means using the same procedure, with ‘O-M’ replaced by corresponding Aqua and Terra ‘subskin’  $\Delta T_{\text{S}}$ .

Figure 14 shows the Terra–Aqua nighttime ‘O-M’ DDs for all TEBs used by ACSPO and the corresponding  $\Delta T_{\text{S}}$ . The results are shown for the original and detrended BTs. Figure 14a shows that a positive Terra–Aqua ‘O-M’ DD trend in band 20 of  $+0.026$  K/decade lasted until the end of 2011. Based on the excellent stability of the Terra nighttime SST and the downward Aqua SST trend vs. various in situ SSTs shown in Figure 12a,c,e,g, we attribute the band 20 calibration drift to Aqua. After 2011, a larger  $+0.040$  K/decade BT drift in band 20 is attributed to Terra, based on the stable Aqua SST and upward trend in the Terra nighttime SST (see Figure 12a,c,e,g) during this period.



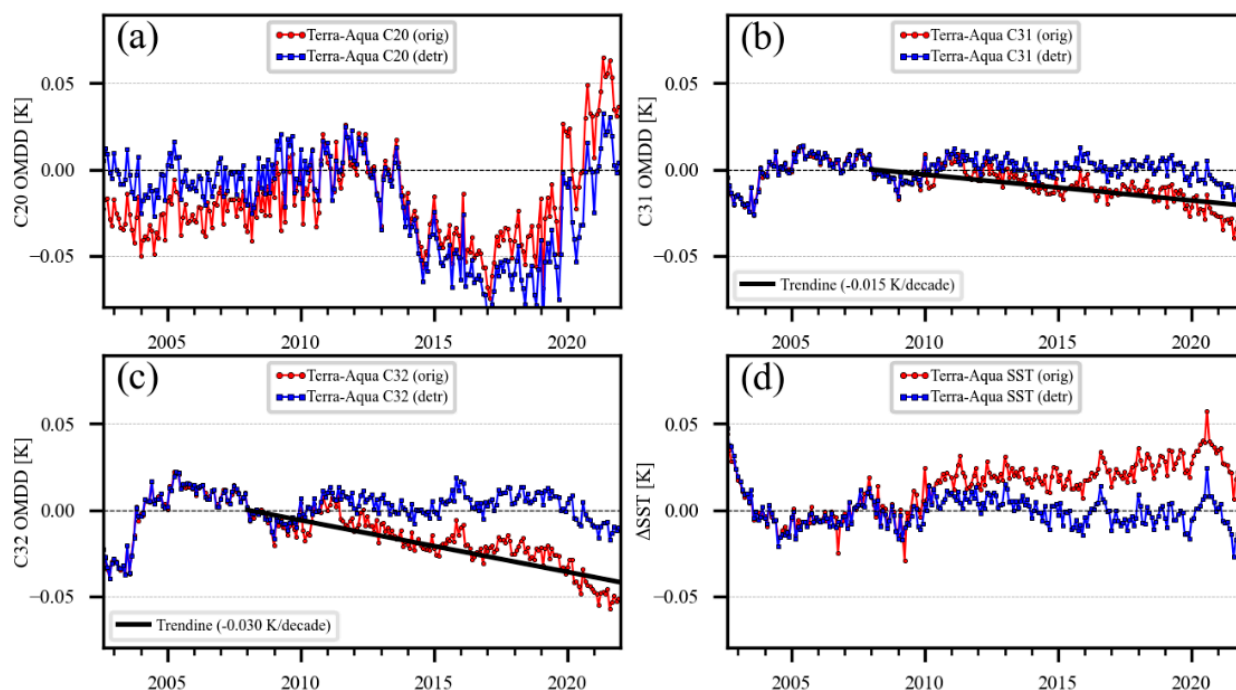
**Figure 14.** (a–c): Monthly aggregated global mean nighttime Terra–Aqua ‘O-M’ DDs for (a) MWIR and (b,c) LWIR bands used in ACSPO; (d): corresponding global mean difference in the Terra and Aqua nighttime ‘subskin’  $\Delta T_{\text{S}}$ . (Blue) detrended and (red) original MODIS BTs. Black and gray lines show the linear trends obtained from the original (uncorrected) MODIS ‘O-M’ DDs. Seasonal signals in Terra–Aqua ‘O-M’ DDs/ $\Delta T_{\text{S}}$  due to different Aqua and Terra orbits, have been subtracted using the STL algorithm [39]. For easier viewing, the mean ‘O-M’ DDs/ $\Delta T_{\text{S}}$  are offset vertically with the convention that the detrended results are centered at zero.

Figure 14b,c show the Terra–Aqua ‘O–M’ DDs for LWIR bands 31 and 32. Both show negative drifts of  $-0.015$  K/decade and  $-0.030$  K/decade, respectively. These bands are only used during the daytime, and they define the stability of the ACSPO daytime SSTs. During this period, the Terra daytime ‘subskin’  $\Delta T_S$  had a noticeable upward trend vs. various in situ SSTs (cf. Figure 13a,c,e,g), while the corresponding Aqua  $\Delta T_{SS}$  were more stable. Based on the stability of the Aqua daytime SST, we attribute the ‘O–M’ DD drift to negative drifts in Terra bands 31 and 32. It might appear counterintuitive that negative drifts in both bands 31 and 32 are inverted, and result in a positive trend in  $\Delta T_S$ . However, the magnitude of the band 32 trend is doubled compared to that of band 31, and its load on the daytime SST is negative (see Table 1), resulting in a net positive  $\Delta T_S$  trend.

The BT drift rates and relevant start/end dates for all bands used by ACSPO are listed in Table 6. The net BT change (in kelvin) is equal to the offset and the drift rate multiplied by time (in decades) since the drift start date. The detrended BTs are obtained by subtracting the calculated drift from the original BTs. The choice of the constant offset is arbitrary (it can be absorbed into the constant term of the NLSST). However, we chose the offsets such that the drift was zero at the beginning of the Terra mission and after 2012 for Aqua.

**Table 6.** Estimated drift rates and durations of the MODIS BTs. The results are based on an analysis of the cross-comparison of the Terra and Aqua ‘O–M’ BTs (Figures 14 and 15) and the long-term stability of the MODIS ‘subskin’ SST vs. various in situ SSTs (Figures 12 and 13).

Band	Start	End	Drift Rate K/Decade	Offset K
Terra C20	1 January 2012	-	+0.040	0.000
Terra C31	1 January 2008	-	$-0.015$	0.000
Terra C32	1 January 2008	-	$-0.030$	0.000
Aqua C20	4 July 2002	31 December 2011	$-0.026$	0.025



**Figure 15.** (a–d) Same as in Figure 14 but for daytime.

Figure 15 shows the same results as in Figure 14 but for the day. During the daytime, MWIR band 20 is not used but included in Figure 15a for consistency with Figure 14. During the daytime, diurnal warming present in ‘O’ is not captured in the ‘M’, because the CMC L4 foundation SST [37,43] does not resolve the diurnal cycle. To mitigate this specific of daytime data, the trend lines shown in Figure 15 were calculated using the

nighttime ‘O-M’ DD data from Figure 14 and reused in Figure 15. Figure 15b,c shows that the BT drift calculated using nighttime data, works well during the daytime. Figure 15d shows a significantly improved agreement between Terra and Aqua daytime ‘subskin’  $\Delta T_{SS}$  calculated using detrended BTs in bands 31 and 32. A comparison of the daytime Terra SST against the in situ SST with and without detrended BTs (Figure 13) shows that long-term positive drifts in the Terra daytime SSTs vs. in situ SSTs are mitigated.

For additional validation of the proposed MODIS BT detrending procedure, Figure 16 shows a comparison of the ACSPO MODIS RAN1 Terra (Figure 16a) and Aqua (Figure 16b) nighttime SSTs with the ACSPO ‘subskin’ SST from NPP VIIRS [1,47] and the CCI ‘skin’ SST from the Advanced Along-Track Scanning Radiometer (AATSR) instrument flown onboard Envisat [48,49].

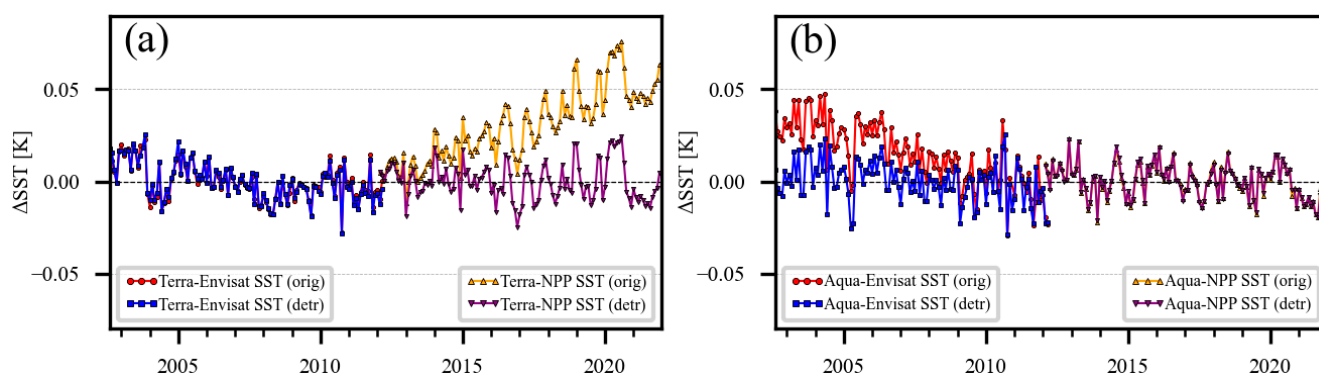


**Figure 16.** Nighttime monthly aggregated global mean MODIS-AATSR  $\Delta T_{SS}$  (June 2002–March 2012) and MODIS-VIIRS  $\Delta T_{SS}$  (February 2012–present) for (a) Terra; (b) Aqua. NPP/VIIRS [47] and MODIS data are ACSPO ‘subskin’ SSTs. AATSR is the ‘skin’ SST from the ESA CCI project [48,49]. Long-term/seasonal signals in  $\Delta T_{SS}$  (due to different satellite orbits, sensor spectral response functions, etc.) have been subtracted using the STL algorithm [39]. For easier viewing, the mean  $\Delta T_{SS}$  are offset vertically to center all detrended mean biases at zero.

The results are shown both with and without detrending of the Terra/Aqua BTs. NPP SST data have been available since 1 February 2012, and the satellite is still active. The NPP flies with a similar afternoon orbit as Aqua, so close agreement between the NPP and Aqua SSTs is expected. The Envisat LEXT ~10 a.m./p.m. suggests a closer agreement with Terra (10:30 a.m./p.m. LEXT). The Envisat AATSR SST was available from July 2002 to April 2012, before contact with the satellite was permanently lost. Figure 16a shows close agreement between the Terra MODIS and AATSR SSTs. The agreement between the Terra MODIS and NPP VIIRS nighttime SSTs improves after the Terra BTs have been detrended. Similarly, Figure 16b shows an improved agreement between the Aqua and Envisat nighttime SSTs prior to 2012, after the Aqua BTs have been detrended. Note that the MODIS BT detrending was performed in this study fully independently from the NPP VIIRS and Envisat AATSR, whose data were analyzed after the MODIS RAN1 datasets had been finalized.

Figure 17 shows the corresponding daytime MODIS RAN1 SST comparisons with VIIRS and AATSR. All time series are noisier than at night, at least in part due to less accurate SST retrievals without a 3.7  $\mu\text{m}$  band. However, the agreement between the MODIS and AATSR daytime SSTs is very strong for both Aqua and Terra, and there is no clear indication of the SST bias drift. The Terra MODIS LWIR bands started drifting in January 2008 (cf. Table 6), so the detrending has a minimal impact on the Terra SST during its overlap with Envisat.

The most prominent feature in Figure 17 is the increasingly positive MODIS SST bias against NPP VIIRS. In previous work, we demonstrated that the NPP daytime SST drift is due to drift in the VIIRS LWIR band calibration [1]. Correction of the VIIRS daytime SST drift will be the subject of the next version of VIIRS Reanalysis (RAN4).

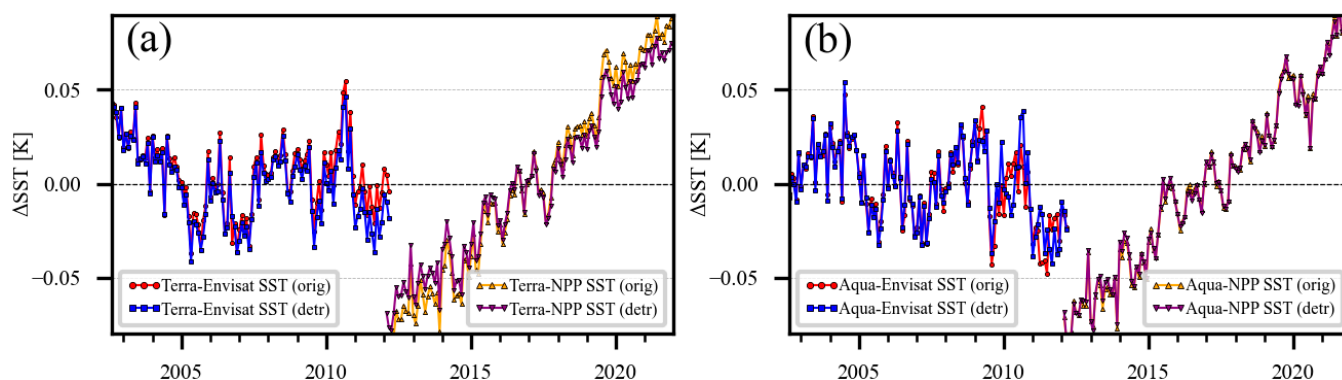


**Figure 17.** (a,b) The same as in Figure 16, but for the daytime SST. See Figure 16’s caption for more details.

## 6. Conclusions

A global 1 km resolution 1st MODIS Reanalysis (RAN1) SST dataset was produced at NOAA using its enterprise Advanced Clear Sky Processor for Ocean (ACSPO) version 2.80 system, for the full Terra (24 February 2000—on) and Aqua (4 July 2002—on) missions. The MODIS RAN1 complements two other existing ACSPO v2.80 RANs: from VIIRs flown onboard 3 JPSS satellites (NPP from February 2012—on; N20 from January 2018—on, and N21 from March 2023—on), and AVHRR FRACs flown onboard 3 Metop-FG satellites -A (December 2006–November 2021), -B (October 2012—on), and -C (December 2018—on) [1,2]. Two SST products are available in ACSPO v2.80 files, ‘subskin’ and ‘depth’. The locations and intensity of thermal fronts are also reported.

A comparison of MODIS SSTs with quality-controlled in situ SSTs from drifters and tropical moorings (DTMs) and Argo floats (AFs) from the NOAA iQuam system shows that MODIS RAN1 SSTs are of high and uniform quality, and consistent across Terra and Aqua. They meet the NOAA JPSS specs for accuracy (global mean bias with respect DTM  $< \pm 0.2$  K) and precision (corresponding global standard deviation  $< 0.6$  K), and often exceed them by a wide margin. This performance is achieved in a clear-sky domain (fraction of clear ice-free ocean pixels in sensor view) of 19.1–20.6%. Estimates of the  $\Delta T_S = T_{SAT} - T_{IS}$  stability vs. the in situ SST were performed. At night, the Aqua and Terra SSTs agree very closely. The corresponding drifts relative to the TMs do not exceed  $\pm 0.01$  K/decade, for both the ‘subskin’ and ‘depth’ SSTs. During the daytime, drifts in the ‘depth’ SSTs are again within  $\pm 0.01$  K/decade, whereas for the ‘subskin’ SST a positive drift of  $\sim +0.02$  K/decade is seen for both Aqua and Terra. All estimates are well within the (A)ATSR Reprocessing for Climate (ARC) project target stability of 0.05 K/decade [36].

Achieving these high standards of performance required some corrections and adjustments to the MODIS brightness temperatures (BTs), in particular, for Terra, which were addressed in RAN1. Two steps in mid-wave infrared (MWIR) BTs in bands 20, 22, and 23, were related to changes in the Terra MODIS operating configuration. If not accounted for, these BT steps result in three epochs of nighttime SSTs, each of which is stable, but with  $\sim 0.1$  K inconsistencies between configuration changes. The steps in Terra MODIS MWIR calibration and their effects on nighttime SSTs were previously reported in [8]. The authors mitigated those by training separate SST retrieval coefficients for each epoch. This approach may not be optimal due to the relative scarcity of in situ training data in the early 2000s and the short durations of the first two epochs (less than a year each). In MODIS RAN1, those were mitigated by estimating the BT discontinuities from the time series of the global mean observed minus modeled (‘O-M’) BT biases, and those offsets were used to debias the Terra MODIS L1b BTs in MWIR bands 20, 22, and 23.

During the early evaluation, we observed artifacts in the Terra nighttime SSTs, concurrent with changes in the MODIS nominal BBT during quarterly warm-up cool-down (WUCD) events, when a positive  $\sim 0.1$  K global daily mean biased were observed (Appendix B). In MODIS RAN1, these steps were mitigated by computing the ‘O-M’ BT

bias dependency on blackbody temperature (BBT) anomalies (deviation from the nominal temperature). Estimated corrections were applied to Terra MODIS thermal emissive bands (TEBs). The MWIR bands are more affected than the longwave infrared (LWIR) bands, which explains the much smaller SST artifacts during the daytime. We also identified and corrected discontinuities in the MWIR BTs, when the Terra MODIS nominal BBT changed from 290 to 285 K on 25 April 2020. If not accounted for, this step in the BTs results in a positive  $\sim 0.05$  K step in the nighttime ‘subskin’ SST. We did not observe Aqua MODIS calibration artifacts related to BBT variations during WUCDs.

Initial checks of the stability of the MODIS SSTs demonstrated drift on the order of 0.025 K/decade against various in situ SSTs over the course of both Terra and Aqua missions. An analysis of the Aqua and Terra MODIS observed minus modeled (‘O-M’) BTs and cross-comparisons with SST trends enabled us to identify and estimate calibration drifts in MODIS TEBs. We used the estimated drifts to detrend MODIS L1b data and confirmed the improved stability of the ACSPO MODIS RAN1 SST. The presence of the drifts in the original MODIS data and the efficacy of their correction in present work were independently confirmed by comparisons with Envisat AATSR and NPP VIIRS SSTs.

At the time of writing, the complete archive of Terra and Aqua  $0.02^\circ$  Level 3 collated data (L3C; two files per 24 h stratified by day and night) is available at NOAA CoastWatch [5]. Due to the large data volume, MODIS RAN1 L2P and L3U data have not yet been archived. Archival of the full MODIS RAN1 dataset, including L2P, L3U, and L3C, will be discussed with NASA PO.DAAC and NOAA NCEI. New data are added in ‘science quality’ delayed mode monthly, with a latency of two months (approximate latency of the availability of MERRA atmospheric profiles [44–46]). Due to the ongoing degradation of the Terra and Aqua orbits and the associated degradation of the SST data quality, new data are not added in near-real-time. For users interested in near-real-time SST data, we recommend JPSS VIIRS and Metop-FG AVHRR FRAC SST data [1,2].

Users interested in a reduced volume, more-information-dense SST data, can use ACSPO  $0.02^\circ$  super-collated family of products from low-Earth-orbiting platforms (L3S-LEO) [14]. The L3S-LEO family includes three lines. The ‘PM’ line from afternoon orbit satellites (in v2.80, NPP and N20); the ‘AM’ line from mid-morning orbit satellites (in v2.80, Metop-A/B/C). The P.M. and A.M. lines each report two files per 24 h, stratified by the day and nighttime viewing conditions. The daily (DY) product combines data from all available ACSPO L3S-LEO a.m./p.m. data, from both day and night, into a single daily file, with the SST normalized at 1:30 a.m. local time viewing conditions (nighttime P.M. orbit).

Extending the L3S-LEO-PM time series from February 2012 (earliest NPP VIIRS SST) back to July 2002 (earliest Aqua MODIS SST) was requested by NOAA users and served as the major motivator and driver for MODIS RAN1. Aqua MODIS SSTs are included in L3S-LEO-PM v2.81, an update from v2.80, which only included VIIRS data. Due to its current orbital drift, Aqua SST data are not included in L3S-LEO-PM v2.81 after 31 December 2022 (see Figure 1). Data from Terra are not included in the A.M. line, due to the significant difference in LEXT (10:30 a.m./p.m.) compared to Metop-FG (9:30 a.m./p.m.). However, Terra SST data are included in the L3S-LEO-DY v2.81 product, and the covered period extends back to 24 February 2000. Due to orbit degradation, Terra is not included in L3S-LEO-DY after 31 December 2021 (see Figure 1). A complete archive of both the L3S-LEO-PM and L3S-LEO-DY v2.81 products, which include MODIS, is available at NOAA CoastWatch [14] succeeding the previous v2.80 datasets. Archival of L3S-LEO v2.81 at PO.DAAC is underway.

Future ACSPO MODIS work will include the mitigation of Aqua and Terra orbit drift on the retrieved SSTs. The last (non-collision avoidance) orbit maintenance maneuvers were performed on 27 February 2020 for Terra and on 19 March 2021 for Aqua. Since then, the Aqua and Terra LEXTs have been drifting from their nominal 1:30 a.m./p.m. and 10:30 a.m./p.m. times, respectively. As of the time of writing, the LEXTs have only drifted by about 10 min for Aqua and 20 min for Terra, and the effects on the retrieved SSTs are still relatively small when validated against in situ SSTs (see Section 4).

Future work will also involve improvements to the ACSPO Clear-Sky Mask (ACSM) to reduce cloud leakage and over-screening and improve the SST algorithms. The ACSPO v2.80 night-time SST algorithm used for RAN1 employs a traditional multi-band NLSST algorithm, which uses one MWIR band (20) at 3.7  $\mu\text{m}$  and two LWIR bands (31 and 32) at 11 and 12  $\mu\text{m}$ , respectively. A similar SST algorithm was used for ACSPO AVHRR FRAC [2], and a slightly revised algorithm that additionally includes the VIIRS band M14 at 8.6  $\mu\text{m}$ , was used for VIIRS SST retrievals [1]. The authors of [8] reported an improved MODIS nighttime SST performance with a MODIS-unique two-band nighttime SST4 algorithm that employs only two MWIR bands (22 and 23) at 3.9 and 4.0  $\mu\text{m}$ . These bands may be additionally explored in future MODIS RANs.

**Author Contributions:** Conceptualization, O.J. and A.I.; methodology, O.J., A.I., B.P. and V.P.; software, O.J., B.P. and Y.K.; validation, O.J., A.I. and V.P.; formal analysis, O.J., A.I. and V.P.; investigation, O.J., A.I. and V.P.; resources, A.I.; data curation, O.J. and A.I.; writing—original draft preparation, O.J.; writing—review and editing, A.I.; visualization, O.J. and Y.K.; supervision, A.I.; project administration, A.I.; funding acquisition, A.I. All authors have read and agreed to the published version of the manuscript.

**Funding:** This work was supported by the NOAA JPSS Program (Sathya Kalluri, JPSS Program Scientist; Lihang Zhou, JPSS Program Manager; Ingrid Guch, JPSS STAR Manager).

**Data Availability Statement:** The ACSPO MODIS RAN1 dataset is available on NOAA CoastWatch [coastwatch.noaa.gov](https://coastwatch.noaa.gov) (accessed on 20 November 2023). See references for DOIs assigned to specific ACSPO MODIS datasets.

**Acknowledgments:** The authors acknowledge the support of Veronica Lance and Michael Soracco with making the ACSPO MODIS RAN1 data available via the NOAA CoastWatch system. The views, opinions, and findings in this report are those of the authors and should not be construed as an official NOAA or US government position or policy.

**Conflicts of Interest:** Authors Olafur Jonasson, Boris Petrenko, Victor Pryamitsyn and Yuri Kihai were employed by the company Global Science and Technology, Inc. The remaining authors declare that the research was conducted in the absence of any commercial or financial relationships that could be construed as a potential conflict of interest.

## Abbreviations

AATSR	Advanced Along-Track Scanning Radiometer
ACSM	ACSPO Clear-Sky Mask
ACSPO	Advanced Clear-Sky Processor for Ocean
AF	Argo Floats
ARMS	ACSPO Regional Monitor for SST
AVHRR	Advanced Very-High-Resolution Radiometer
BBT	Black Body Temperature
BT	Brightness Temperature
CMC	Canadian Meteorological Centre
CRTM	Community Radiative Transfer Model
DTM	Drifters and Tropical Moorings
DD	Double Difference
FRAC	Full Resolution Area Coverage
GAC	Global Area Coverage
GDS2	Group For High-Resolution SST Data Specification v2
GEO	Geostationary
GHRSSST	Group For High-Resolution SST
iQuam	In situ SST Quality Monitor
JPL	Jet Propulsion Laboratory
JPSS	Joint Polar Satellite System

L1b	Level 1b
L2P	Level 2 Pre-processed
L3C	Level 3 Collated
L3S	Level 3 Super-collated
L3U	Level 3 Uncollated
L4	Level 4
LEO	Low Earth Orbit
LEXT	Local Equator Crossing Times
LWIR	Longwave Infrared
MDS	Matchup Data Set
MERRA	Modern-Era Retrospective Analysis for Research and Applications
Metop	Meteorological Operational Satellite
MODIS	Moderate Resolution Imaging Spectroradiometer
MWIR	Mid-Wave Infrared
N20	NOAA-20
NLSST	Nonlinear Sea Surface Temperature
NOBS	Number Of Observations
NBBT	Nominal Blackbody Temperature
NPP	National Polar-Orbiting Partnership
'O-M'	Observed Minus Modeled
PO.DAAC	Physical Oceanography Distributed Active Archive Center
QL	Quality Level
RAN	Reanalysis
RSD	Robust Standard Deviation
RVS	Response Versus Scan
SD	Standard Deviation
S-NPP	Suomi National Polar-Orbiting Partnership
SQUAM	SST Quality Monitor
SSES	Sensor Specific Error Statistics
SST	Sea Surface Temperature
STL	Seasonal and Trend Decomposition using Loess
TEB	Thermal Emissive Band
TM	Tropical Moorings
VIIRS	Visible Infrared Imaging Radiometer Suite
VZA	View Zenith Angle
WUCD	Warm-Up Cool-Down

### Appendix A. Validation of ACSPO MODIS RAN1 SST against Argo Floats

The NOAA JPSS SST specs for precision and accuracy have been specifically formulated with respect to drifters and tropical moorings (DTMs), not Argo floats (AFs). The reason is that the AFs measure much deeper (~5 m) than DTMs (0.2–1 m) in the layer of the ocean even farther away from where typical satellite infrared measurements sample the ocean surface (~10  $\mu\text{m}$ ). Also, due to their reduced frequency of presence at the ocean surface (~once every 10 days), there are fewer AF matchups compared with DTMs (although the numbers of DTM and AF platforms are comparable), resulting in much noisier validation statistics, as discussed later in this section. In the context of MODIS, the number of AFs in the early 2000s was small and evolved rapidly, further contributing to the non-uniform and noisy validation statistics. Nevertheless, the AFs represent a fully independent and accurate source of in situ data. With some caution and understanding of the underlying physics, they represent a useful additional consistency check and independent verification of satellite SSTs.

The Argo program commenced in 1999 and reached its target of ~3000 active floats in 2008 [38,50]. The number of AFs continued to grow and remained at between 3500 and 4000 since 2016 [15]. Figure A1 shows the time series of the monthly number of MODIS RAN1 matchups with AFs. The NOBS is low in the first years of the Argo program. For this reason, data prior to 2003 have been omitted from all further time series in this Appendix.

The number of matchups remained quite stable in the 2010s but continued to be two orders of magnitude smaller compared to the DTM NOBS (cf. Figure 4).

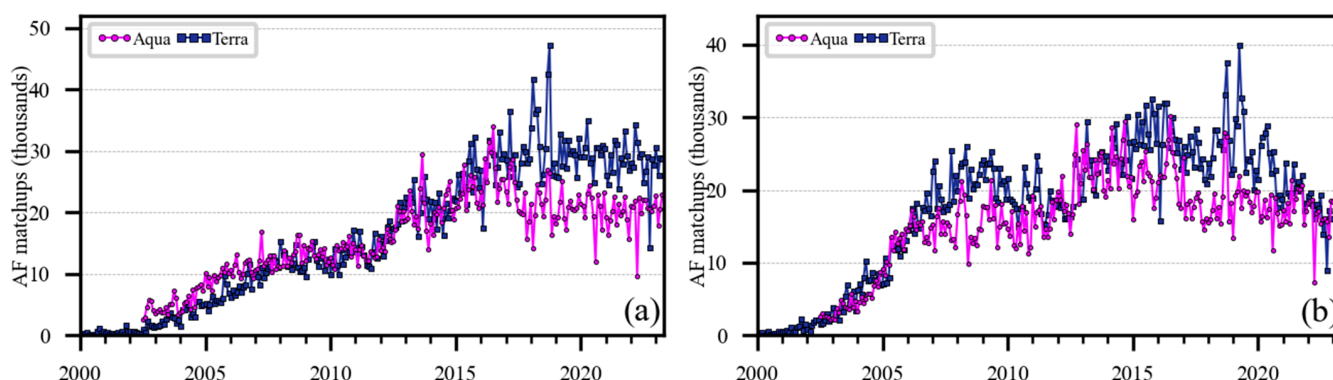


**Figure A1.** Time series of the monthly aggregated number of MODIS RAN1 SST matchups with AFs during the (a) day; and (b) night. Data are from the NOAA SQUAM online system [34].

In contrast to the DTMs, there are noticeable differences in the number of matchups between Aqua and Terra. There are also significant differences between night (Figure A1a) and day (Figure A1b). This is because the AFs do not report data in regular (e.g., hourly) intervals, like DTMs, and the number of their observations depends on the local time. For example, since 2017, there have been noticeably more AF observations at around 10:30 p.m. (Terra night overpass) compared to 1:30 a.m. (Aqua night overpass). As a result, there are more AF matchups from Terra than from Aqua ( $3 \times 10^4$  vs.  $2 \times 10^4$  monthly matchups).

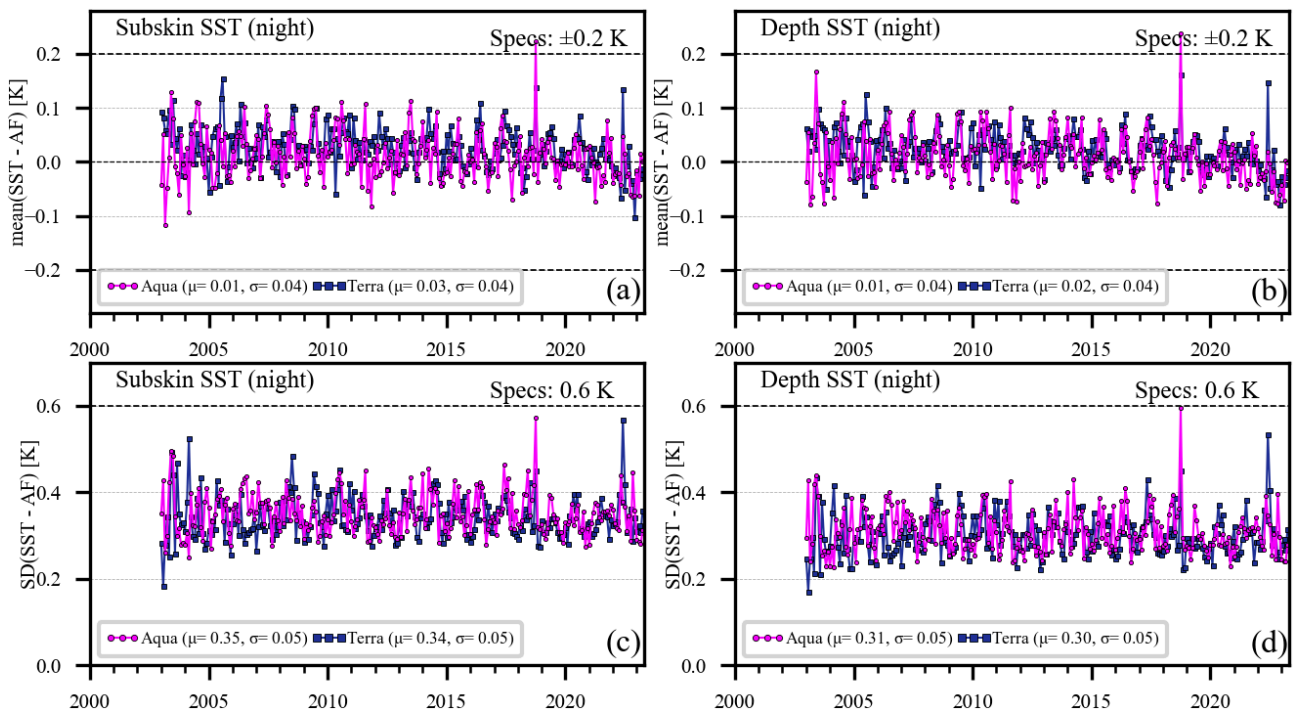
Figure A2 shows the monthly aggregated time series of the global mean biases and standard deviations of the RAN1 night-time ‘subskin’ and ‘depth’ SSTs vs. AFs. They are noisier compared to the DTM time series in Figure 5 due to the NOBSs being two orders of magnitude lower. Overall, the global statistics remain comparable to those for DTMs. Biases are close to zero and are typically within  $\pm 0.1$  K, with several occasional outliers. The global standard deviations ( $\sim 0.34$ – $0.35$  K for ‘subskin’ and  $\sim 0.30$ – $0.31$  K for ‘depth’ SSTs) are  $\sim 0.01$ – $0.03$  K larger compared to those of the DTMs due to their deeper depths ( $\sim 5$  m) compared with the DTMs  $\sim 0.2$ – $1.0$  m and the larger contributions from the variable diurnal thermocline.

Figure A3 shows the corresponding AF validation time series for the daytime SSTs (cf. DTM time series in Figure 6). The month-to-month noise is now strongly intermingled with the seasonal cycle, which is clearly seen in the DTM data.

Both the ‘subskin’ and ‘depth’ SSTs are biased warm relative to the AFs by  $\sim +0.1$  K for Terra and by  $\sim +0.2$  K for Aqua. This is due to diurnal warming, which affects the ‘subskin’ and ‘depth’ SSTs from the mid-morning Terra and afternoon Aqua differently when compared with the AF data at a  $\sim 5$  m depth.

The standard deviations are also increased compared to both night data in Figure A2 and DTM daytime data in Figure 6, more so for the afternoon Aqua, with occasional spikes exceeding 0.8 K. These outliers are significantly reduced in ‘depth’ SSTs. The increased noise and outliers are due to the strong and variable diurnal warming present at the time of Aqua overpass ( $\sim 1:30$  p.m. local time). Note that the degraded daytime validation statistics against AFs are in no way an indication of degraded Aqua ‘subskin’ and ‘depth’ SSTs, but rather, represent the limitation of using the 5 m deep AFs to validate much shallower satellite SSTs.

Table A1 summarizes the ACSPO MODIS RAN1 validation statistics against AFs using the same period as used in Section 4.1 against DTMs (cf. Table 3). At night, the AF statistics are qualitatively and even quantitatively comparable to the corresponding DTM statistics. During the daytime, the AF statistics are particularly degraded and noisy, as expected, but they are included in Table A1 for completeness.



**Figure A2.** Times series of the monthly aggregated global night-time MODIS RAN1–AF SSTs: (a,b) mean biases; (c,d) corresponding standard deviations (SDs); (a,c) ‘subskin’; (b,d) ‘depth’ SST. Temporal means and standard deviations of the time series are given by  $\mu$  and  $\sigma$ , respectively. Dates prior to 1 January 2003 are omitted due to the low NOBS. Data are taken from the NOAA SQUAM online system [34].

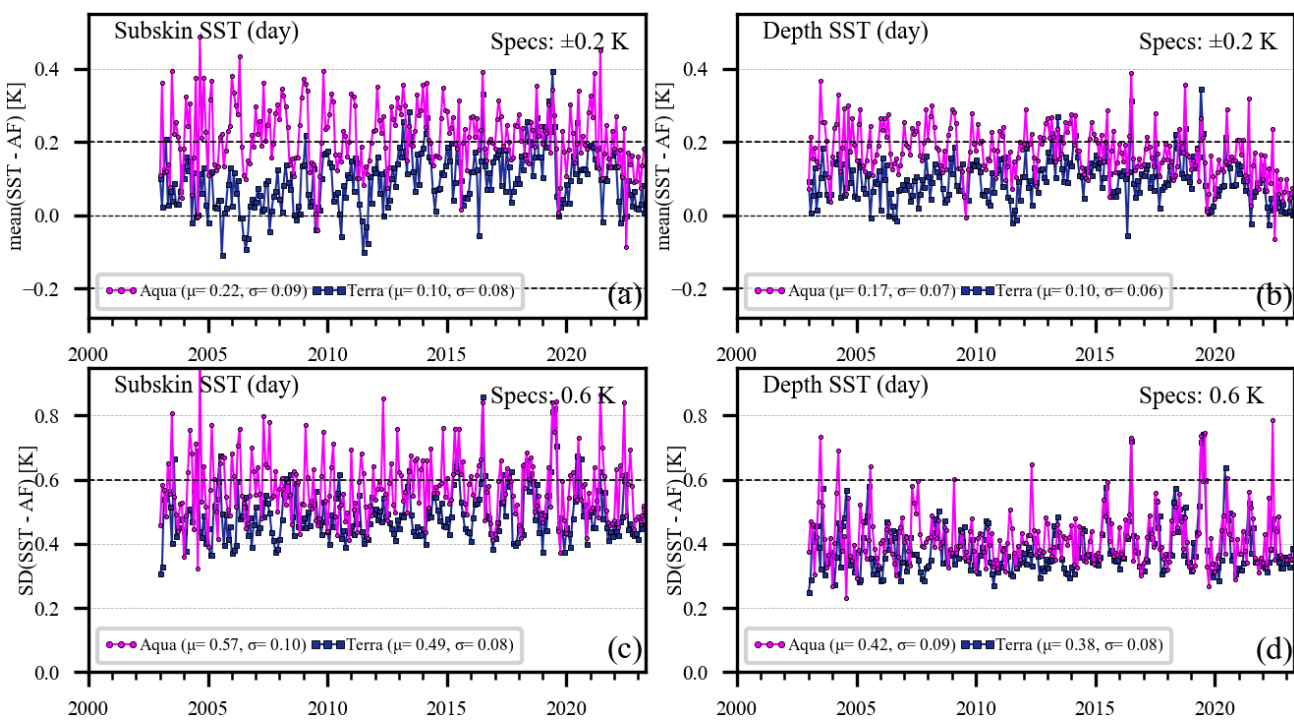


**Figure A3.** (a–d) The same as in Figure A2, but for daytime.

The major observations from Table A1 are consistent with those with respect to DTMs in Table 3. The ACSPO validation statistics remain comparable between MODIS and VIIRS. The standard deviations (SDs) and robust standard deviations (RSDs) are smaller for ACSPO compared to the NASA SSTs, with  $\sim 0.10$  K ( $\sim 0.02$  K) margins. In contrast to

ACSPO, where the ‘depth’ statistics are always improved over the ‘subskin’ data, the SSES bias correction does not improve the performance of NASA SSTs, making the gap between the ACSPO and NASA ‘depth’ SSTs wider.

**Table A1.** Same as in Table 3 except for the AFs.

	SST Product	Mean Subskin	Mean Depth	Median Subskin	Median Depth	SD Subskin	SD Depth	RSD Subskin	RSD Depth	NOBS $\times 10^3$	CSR %	Pixels $\times 10^9$
Night	ACSPO Terra	+0.02	+0.01	+0.05	+0.03	0.32	0.28	0.24	0.19	350	20.6	16.5
	ACSPO Aqua	+0.01	+0.00	+0.03	+0.00	0.33	0.29	0.25	0.20	248	19.1	15.3
	ACSPO NPP	−0.02	−0.03	+0.01	−0.02	0.32	0.33	0.22	0.19	803	18.8	47.9
	ACSPO N20	+0.00	−0.02	+0.02	−0.01	0.33	0.30	0.23	0.22	777	18.8	47.9
	NASA Terra	−0.07	−0.02	−0.10	+0.04	0.42	0.42	0.27	0.26	307	17.7	14.2
	NASA Aqua	−0.13	−0.05	−0.17	−0.01	0.41	0.41	0.26	0.27	215	16.3	13.1
Day	ACSPO Terra	+0.17	+0.13	+0.12	+0.09	0.59	0.49	0.42	0.32	325	19.3	15.7
	ACSPO Aqua	+0.20	+0.14	+0.13	+0.09	0.61	0.48	0.41	0.30	224	20.4	16.6
	ACSPO NPP	+0.15	+0.15	+0.07	+0.09	0.61	0.45	0.38	0.29	777	19.8	51.2
	ACSPO N20	+0.16	+0.17	+0.07	0.48	0.63	0.48	0.38	0.30	755	20.0	51.4
	NASA Terra	+0.13	+0.13	+0.09	+0.09	0.66	0.67	0.47	0.47	380	22.6	18.4
	NASA Aqua	+0.13	+0.10	+0.08	+0.08	0.63	0.63	0.43	0.42	253	22.6	18.5

## Appendix B. Mitigation of Terra BT Artifacts Due to Variations in the Blackbody Temperature

At the initial stages of the Terra RAN1, anomalies were observed in the retrieved SSTs when MODIS blackbody temperature (BBT) deviated from its nominal value. There are two types of such anomalies: (1) when the BBT was varied during quarterly warm-up cool-down (WUCD) exercises and (2) the permanent change in the nominal Terra MODIS BBT from 290 to 285 K on 25 April 2020.

### Appendix B.1. Mitigation of BT Anomalies During Warm-Up/Cool-Down (WUCD) Events

During the WUCD events, the MODIS BBT is varied between the ambient instrument temperature ( $\sim 272$  K) and 315 K, with the goal being to characterize the TEB response and radiometric noise [40]. Figure A4a shows evolution of the BBT during a typical WUCD exercise on 18–21 September 2009. Customarily, WUCDs are performed quarterly for both MODIS instruments, and each exercise lasts about 3 days [51]. For most of the WUCD cycle, the BBT is below its nominal value, as is also confirmed by Figure A4b, which illustrates the frequency of various BBT anomalies during the WUCDs.

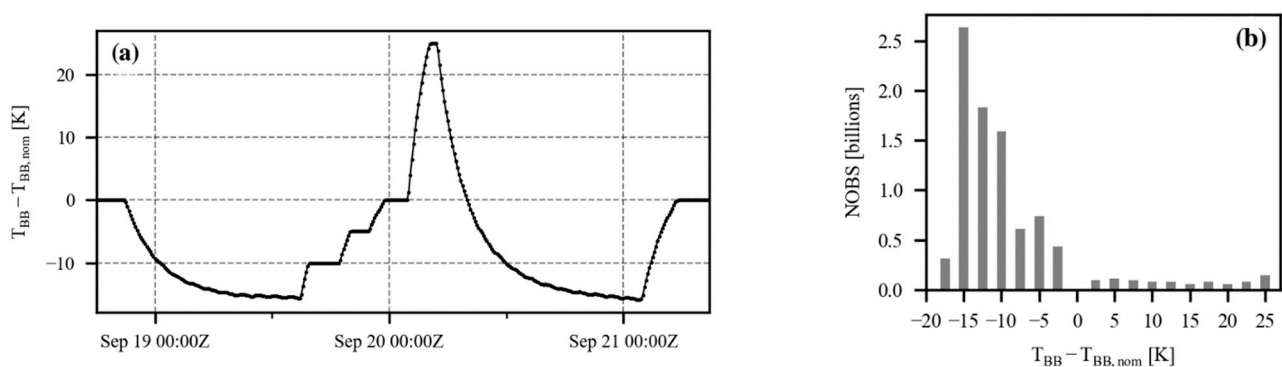


**Figure A4.** (a) Terra MODIS BBT anomaly  $\Delta T_{BB} = T_{BB} - T_{BB,nom}$  (nominal BBT,  $T_{BB,nom} = 290$  K) during one WUCD exercise on 18–21 September 2009. Each data point represents an average  $\Delta T_{BB}$  with 10 min intervals. (b) Histogram showing the number of clear-sky MODIS-T L2P observations (NOBS) as a function of the BBT anomaly during all WUCD exercises from 3 July 2001 to 25 April 2020 (from the onset of AA2 configuration to the time when the nominal BBT was changed to 285 K). Observations with  $\Delta T_{BB}$  near 0 K are not shown in the histogram to avoid the saturation of the  $y$ -axis.

At the early stages of MODIS RAN, we observed systematic  $\sim 0.1$  K warm nighttime SST anomalies concurrent with WUCD events. They are specific to Terra (not observed for Aqua) and are only seen in nighttime SSTs, suggesting that the degraded calibration of Terra MODIS MWIR BTs is the cause.

Figure A5 shows 24 h aggregated global mean daily biases for the ACSPO and NASA night-time SSTs against the CMC L4 foundation SST [37,43] for two representative years, 2009 (nominal BBT = 290 K) and 2021 (nominal BBT = 285 K). The SST spikes reaching  $\sim +0.1$  K are well beyond the day-to-day noise in the time series and are clearly seen in both the ACSPO (before WUCD mitigation) and NASA MODIS SSTs during all five Terra MODIS WUCD exercises performed in 2009. In 2021, spikes are also seen, but with the magnitudes reduced approximately by half. (The cause will be discussed later). In comparison, Figure A5 also shows the time series from the final MODIS RAN1, i.e., that calculated using WUCD-corrected BTs with the model described later in this section.

The fact that WUCD SST anomalies are not prominent during the daytime suggests that the MWIR bands are the main cause. LWIR SST bands 31 and 32, which are used in the ACSPO nighttime algorithm, may also contribute, but likely to a lesser extent. (Recall also that the NASA SST4 night-time algorithm relies on bands 22 and 23 centered at 3.9 and 4.0  $\mu\text{m}$ , but still shows spikes of similar magnitudes).

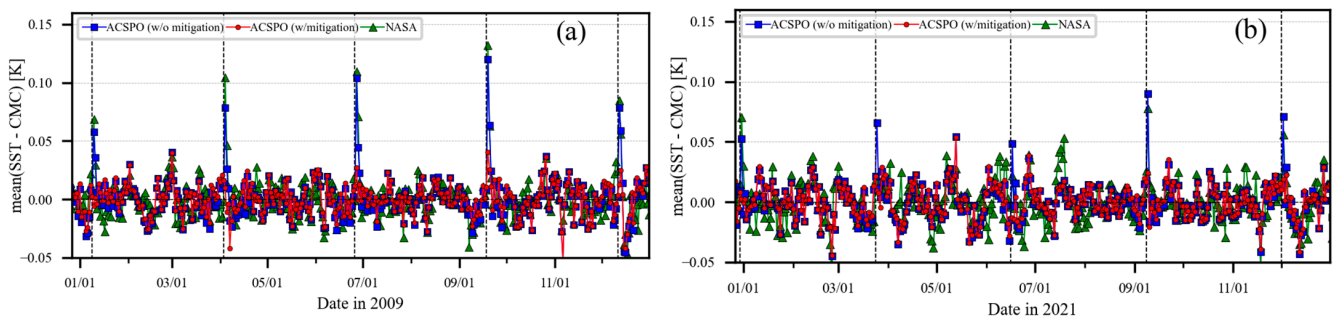


**Figure A5.** Time series of 24 h aggregated global mean biases,  $\Delta T_S = \text{ACSPO 'subskin'—CMC L4 foundation SST bilinearly interpolated to the MODIS native grid: (blue squares) without and (red circles) with WUCD anomaly mitigation. The corresponding mean biases for NASA SSTs are also shown. A } \pm 15$  day running average was subtracted from the time series to remove slow seasonal variations and to normalize the  $y$ -axis to  $\sim 0$  K to facilitate comparisons of the NASA 'skin' and ACSPO 'subskin' SST products. (a) Results for the year 2009, when the nominal BBT was set at 290 K and five WUCD exercises were performed (with beginning dates of 9 January, 3 April, 26 June, 18 September, and 11 December; denoted by vertical dashed lines). (b) Similar results, but for the year 2021, when the nominal BBT was set at 285 K and five WUCD exercises were performed (with beginning dates of 30 December 2020 and 24 March, 16 June, 8 September, and 1 December 2021; denoted by vertical dashed lines).

To mitigate the WUCD-induced SST anomalies, we performed an empirical correction of MODIS BTs based on variations in the observed minus the modeled 'O-M' BT biases during WUCD cycles (using CRTM version 2.3.0 [16–18], informed by MERRA-2 and CMC L4 foundation SSTs [37,43–46]). The 'O-M' biases were computed over multiple WUCDs and stratified by the BBT anomalies,  $\Delta T_{BB}$ . In order to minimize the effects of long-term trends (e.g., seasonal) in the 'O-M' statistics, they were calculated for an additional 24 h before and after each WUCD cycle to establish a 'baseline' for the WUCD in close proximity. The 'O-M' BT dependencies for each band were approximated by piecewise linear functions of the form

$$B_{WUCD}(\Delta T_{BB}) = \begin{cases} B_L & \text{if } \Delta T_{BB} < T_L \\ B_L \frac{\Delta T_{BB} - T_1}{T_L - T_1} & \text{if } T_L \leq \Delta T_{BB} < T_1 \\ 0 & \text{if } T_1 \leq \Delta T_{BB} < T_2 \\ B_H \frac{\Delta T_{BB} - T_2}{T_H - T_2} & \text{if } T_2 \leq \Delta T_{BB} < T_H \\ B_H & \text{if } \Delta T_{BB} > T_H \end{cases} \quad (A1)$$

Here,  $T_i$  ( $i = L, H, 1, 2$ ) and  $B_j$  ( $j = L, H$ ) are fitting parameters with ( $T_L < T_1 \leq 0 \leq T_2 < T_H$ ), which were chosen by visual inspection of the ‘O-M’ BT bias dependency on the BBT anomaly. Equation (A1) describes a piecewise linear function with the following properties:

- Varies linearly from  $B_L$  to zero for values of  $\Delta T_{BB}$  between  $T_L$  and  $T_1$ ;
- Is zero between  $T_1$  and  $T_2$ , where  $T_1 \leq 0 \leq T_2$ . With this convention, the WUCD correction is zero at the nominal BBT ( $\Delta T_{BB} = 0$ );
- Varies linearly from zero to  $B_H$  between  $T_2$  and  $T_H$ ;
- Is constant for  $\Delta T_{BB}$  outside the range  $[T_L, T_H]$ .

The piecewise linear function was chosen because, despite its simple form, it adequately captures the shape of the WUCD biases. We found that the change in the nominal BBT from 290 to 285 K did affect the ‘O-M’ BT biases, so we split our analyses into two periods corresponding to two nominal BBTs. The analyses were performed for all MODIS bands used for SST retrievals in either the ACSPO algorithm or the NASA SST algorithm. For completeness, band 29 centered at 8.6  $\mu\text{m}$  was also included. (Recall that, currently, it is not used in either the ACSPO or NASA retrievals due to a degraded performance [1,27,28]).

‘O-M’ BT biases measured as a function of the BBT anomaly are shown in Figure A6 for all SST bands for the nominal BBT of 290 K. The model results obtained using Equation (A1) are also overlaid. Table A2 lists the model parameters. BT biases clearly vary with the BBT in all SST bands. The dependencies are more pronounced in MWIR than in the LWIR bands, explaining why the WUCD effects are more apparent for the nighttime SST, as discussed earlier in this section. The effect is larger for negative  $\Delta T_{BB}$ s (recall that for the majority of the time during a WUCD cycle,  $\Delta T_{BB}$ s are negative; cf. Figure A4b). The MWIR biases are always positive, whereas in the LWIR bands, they are smaller in magnitude and have opposite signs for negative and positive  $\Delta T_{BB}$ s.

The opposite bias signs for positive and negative  $\Delta T_{BB}$ s explains the overall lower effect of WUCDs on the daytime SSTs. MWIR BT biases are more pronounced in bands 22 and 23 used in the NASA nighttime SST4, compared to band 20 used by the ACSPO night-time SST. This is consistent with the larger WUCD SST anomalies in the NASA SST4 product, as shown in Figure A5a. By far the largest WUCD BT biases are observed in band 29 (note the significantly larger vertical axis range in Figure A6d). However, this band is not used in ACSPO or NASA SST products and is only included in these analyses for completeness.

Figure A7 shows the same results as in Figure A6, but for a period after the nominal BBT on Terra was changed from 290 K to 285 K.

For the MWIR bands, the shapes, magnitudes, and even the signs of the WUCD biases are substantially different. For positive  $\Delta T_{BB}$ s, the MWIR BT biases are negative. For positive  $\Delta T_{BB}$ s, they are significantly reduced in magnitude in bands 22 and 23, while no change was observed in band 20. Based on the reduced BT biases for bands 22 and 23 (used in NASA SST4) and the opposite signs for the positive/negative  $\Delta T_{BB}$ s, we expect SST anomalies during the WUCD exercises to be reduced in magnitude after the nominal BBT change, especially for the NASA SST4 product. This is consistent with the time series of the global mean ACSPO and NASA SST4 bias against the L4 SST for the year 2021 (Figure A5b), which are noticeably reduced compared to the 2009 results (Figure A5a). The WUCD BT biases in LWIR SST bands 31–32 (Figure A7e,f) show similar behaviors after the nominal BBT changed, but their magnitudes decrease for negative  $\Delta T_{BB}$ s and increase

for positive  $\Delta T_{BBs}$ . However, the increased BT bias for positive  $\Delta T_{BBs}$  did not result in a noticeable increase in the WUCD SST anomalies during the daytime, most likely due to the small fraction of the WUCD cycle duration spent at a positive  $\Delta T_{BB}$ . For band 28 (not used for SST), the shape of the WUCD BT bias in Figure A7d remains unchanged, but the magnitude is approximately doubled and reaches  $\sim 0.6$  K during the warmest phase of the WUCD cycles.

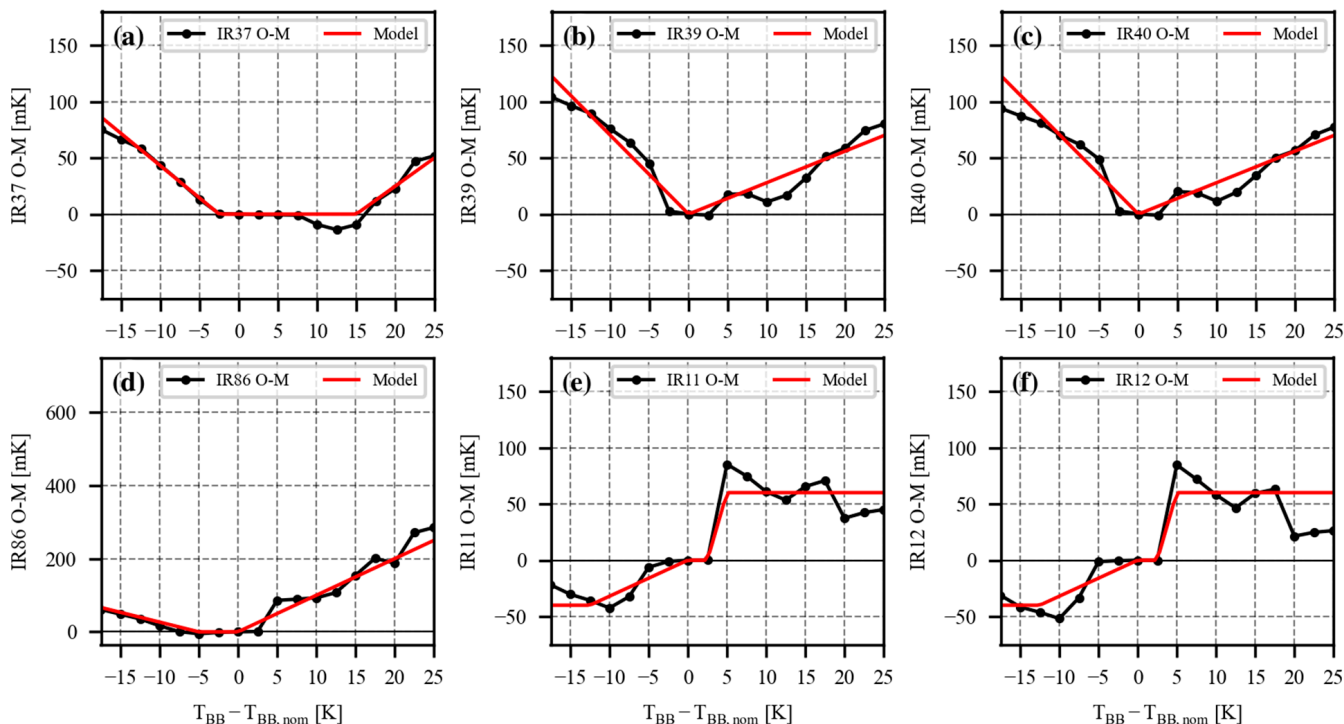


**Figure A6.** ‘O-M’ BTs stratified by the BBT anomaly for Terra MODIS (top) MWIR and (bottom) LWIR bands (a) 20 (3.7  $\mu\text{m}$ ), (b) 22 (3.9  $\mu\text{m}$ ), (c) 23 (4.0  $\mu\text{m}$ ), (d) 29 (8.6  $\mu\text{m}$ ), (e) 31 (11  $\mu\text{m}$ ), and (f) 32 (12  $\mu\text{m}$ ). Black dotted curves: clear-sky ‘O-M’ BTs from all WUCD cycles from 3 July 2001 to 25 April 2020 (last date before the MODIS nominal BBT was changed from 290 to 285 K). Red curves: model results using Equation (A1) with the coefficients listed in Table A2. See text for more details.

**Table A2.** Values of the parameters used in Equation (A1) for all considered SST bands. Parameter values are provided for periods with the Terra MODIS nominal BBT (NBBT) of 290 K (mission start–25 April 2020) and 285 K (after 25 April 2020). All parameters are in units of Kelvin.

	Band	$B_L$	$B_H$	$T_L$	$T_1$	$T_2$	$T_H$
290 K NBBT	20	0.10	0.05	−20.0	−2.5	15.0	25.0
	21	0.14	0.07	−20.0	0.0	0.0	25.0
	22	0.14	0.07	−20.0	0.0	0.0	25.0
	29	0.08	0.25	−20.0	−5.0	0.0	25.0
	31	−0.04	0.06	−12.5	0.0	2.5	5.0
	32	−0.04	0.06	−12.5	0.0	2.5	5.0
285 K NBBT	20	0.07	−0.05	−10.0	−2.5	2.5	15.0
	22	0.06	−0.03	−10.0	0.0	0.0	15.0
	23	0.06	−0.02	−10.0	0.0	10.0	20.0
	29	0.08	0.55	−10.0	−2.5	10.0	30.0
	31	−0.02	0.08	−10.0	0.0	2.5	5.0
	32	−0.02	0.08	−10.0	0.0	2.5	5.0

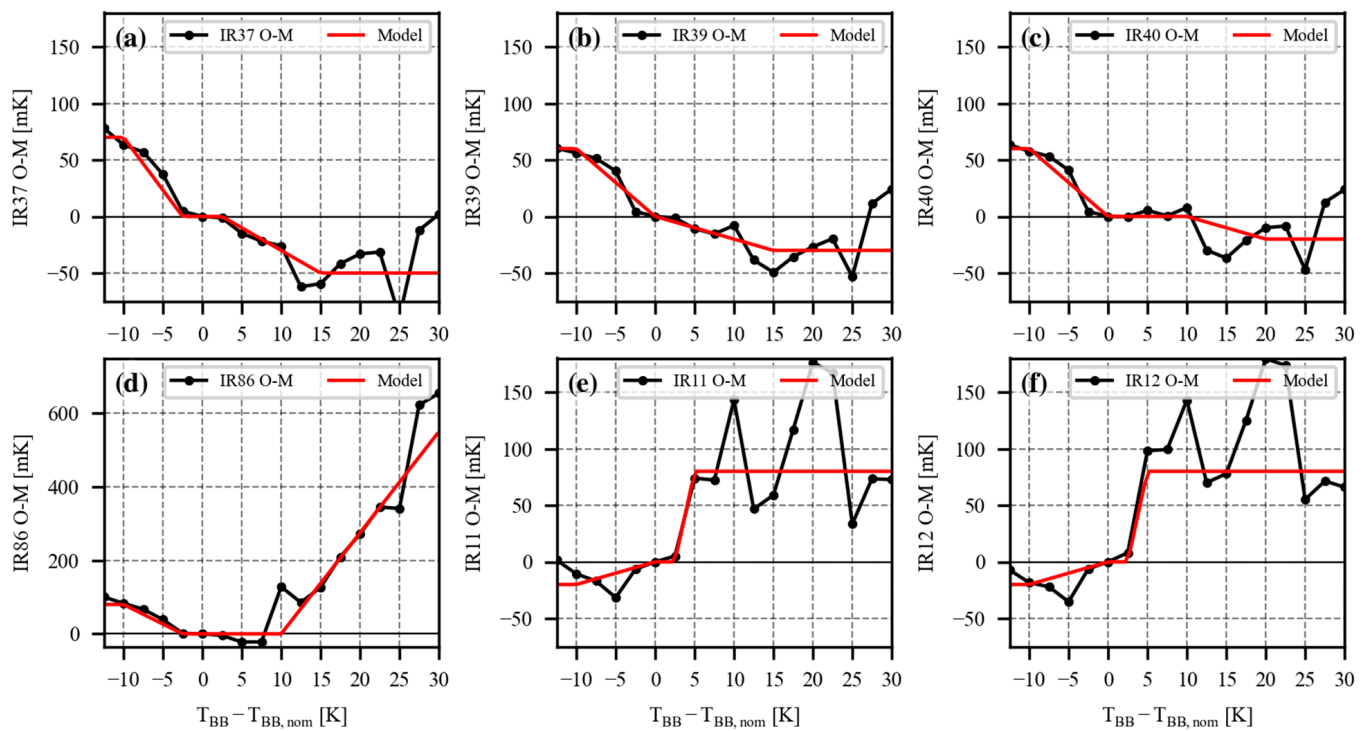


**Figure A7.** (a–f) The same as in Figure A6, except only for WUCD exercises after the switch to a nominal BBT of 285 K (26 April 2020–31 December 2022).

#### Appendix B.2. Mitigation of SST Anomalies Due to Changes in the Nominal BBT

For the majority of the Terra mission, the nominal BBT has been kept at 290 K, which is 5 K higher than that for Aqua (285 K; constant for entire mission) [40]. On 25 April 2020, the Terra MODIS nominal BBT was lowered to 285 K following a WUCD exercise on 22–25 April [51]. Concurrent with the change in the nominal BBT, a positive step in the nighttime ‘subskin’ SST of  $\sim +0.04$  K was observed (see Figure A8a). (No analogous step was observed in the daytime SST). Corresponding steps of +0.035 K, +0.054 K, and +0.067 K were observed in the ‘O-M’ BTs in MWIR bands 20, 22, and 23, respectively (see Figure A8b–d). This is a strong indication that the source of the nighttime SST discontinuity was the abrupt change in the MWIR BTs, since band 20 centered at  $3.7 \mu\text{m}$  is the main contributor to the ACSPO night-time SST and is not used during the daytime.

Note that the time series of the satellite SST minus L4 and ‘O-M’ BTs without mitigation (shown in red circles in Figure A8) are not corrected for the WUCD BT biases discussed in the previous section of this appendix. The mitigated results (shown in blue rectangles) are corrected for WUCD calibration artifacts and for the BT discontinuity due to the nominal BBT change. This event was complicated by the fact that the nominal BBT change from 290 to 285 K on 25 April 2020 occurred immediately after the WUCD exercise on 22–25 April 2020. The occurrence of the WUCD exercise prior to the nominal BBT change makes the SST/BTs discontinuity appear to occur on April 23, two days prior to the nominal BBT change on April 25.

To reconcile the SSTs before and after the nominal BBT change, we subtracted the identified ‘O-M’ steps from all Terra MODIS BTs obtained at BBT=285 K. Figure A8 shows that this successfully mitigates discontinuities in the ‘O-M’ BT biases (Figure A8b–d). As a result, the ACSPO nighttime ‘subskin’ SSTs (Figure A8a) are also reconciled, thus providing an independent verification of the correction in band 20.

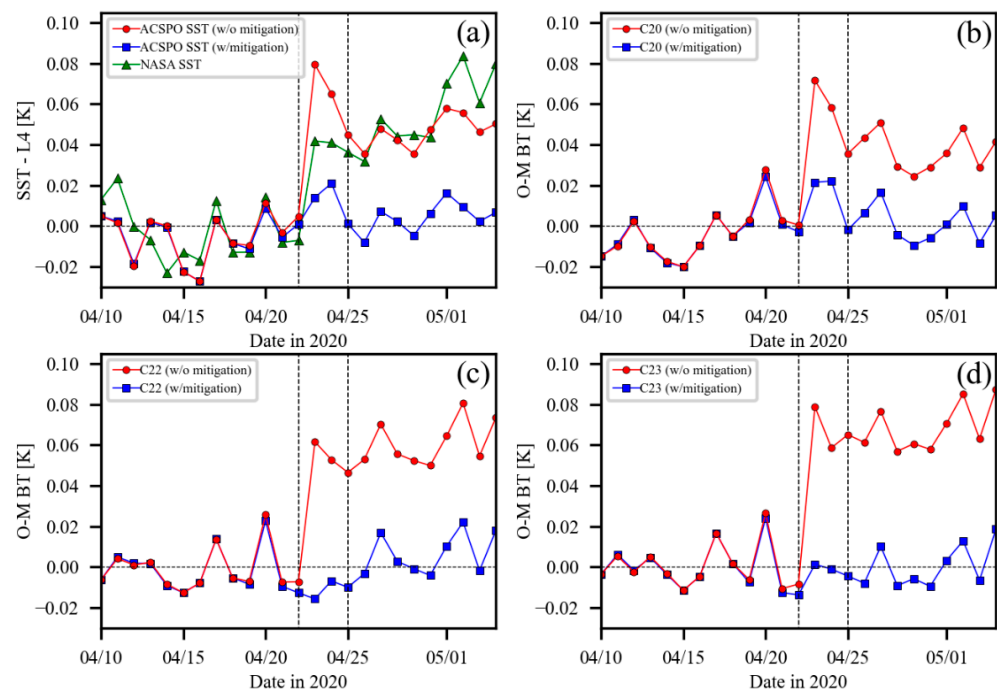


**Figure A8.** Time series of the daily aggregated global mean biases (a)  $\Delta T_s =$  Terra ACSP0 nighttime ‘subskin’ and NASA ‘skin’ SSTs minus the CMC L4 foundation SST. The results are shown with and without BT discontinuity mitigation. Terra MODIS ‘O-M’ BTs in bands (b) 20, (c) 22, and (d) 23. The two vertical dashed lines denote 22 April (start of the WUCD exercise) and 25 April (end of the WUCD exercise and first date with a nominal BBT of 285 K). For ease of viewing, the ACSP0 SST and ‘O-M’ time series are shifted vertically by a constant value, such that the mean bias of the time series with BT discontinuity mitigation is centered at zero. The NASA SST time series were shifted, such that mean bias prior to 22 April is centered at zero. Note that the time series with mitigation have also been corrected for WUCD BT biases in addition to BT discontinuity mitigation.

## References

- Jonasson, O.; Ignatov, A.; Pryamitsyn, V.; Petrenko, B.; Kihai, Y. JPSS VIIRS SST Reanalysis Version 3. *Remote Sens.* **2022**, *14*, 3476. [CrossRef]
- Pryamitsyn, V.; Petrenko, B.; Ignatov, A.; Kihai, Y. Metop First Generation AVHRR FRAC SST Reanalysis Version 1. *Remote Sens.* **2021**, *13*, 4046. [CrossRef]
- MODIS Science Team. MYD021KM MODIS/Aqua Calibrated Radiances 5-Min L1B Swath 1 km. Available online: <https://ladsweb.modaps.eosdis.nasa.gov/missions-and-measurements/products/MYD021KM> (accessed on 12 July 2023). [CrossRef]
- MODIS Science Team. MOD021KM MODIS/Terra Calibrated Radiances 5-Min L1B Swath 1 km. Available online: <https://ladsweb.modaps.eosdis.nasa.gov/missions-and-measurements/products/MOD021KM> (accessed on 12 July 2023).
- ACSP0 Global SST from MODIS | NOAA CoastWatch & OceanWatch. Available online: <https://coastwatch.noaa.gov/cwn/products/acspo-global-sst-modis.html> (accessed on 18 July 2023).
- The Group for High Resolution Sea Surface Temperature Science Team. *The Recommended GHRSSST Data Specification (GDS) 2.0 Revision 5*; GHRSSST International Project Office: Copenhagen, Denmark, 2012. [CrossRef]
- Petrenko, B.; Ignatov, A.; Kihai, Y.; Heidinger, A. Clear-Sky Mask for the Advanced Clear-Sky Processor for Oceans. *J. Atmospheric Ocean. Technol.* **2010**, *27*, 1609–1623. [CrossRef]
- Kilpatrick, K.A.; Podestá, G.; Walsh, S.; Williams, E.; Halliwell, V.; Szczodrak, M.; Brown, O.B.; Minnett, P.J.; Evans, R. A Decade of Sea Surface Temperature from MODIS. *Remote Sens. Environ.* **2015**, *165*, 27–41. [CrossRef]
- Kilpatrick, K.A.; Minnet, P.J.; Luo, B. Validation of NASA MODIS R2019.0 Reprocessed SST Products. GHRSSST XX, 2019, Frascati, Italy. Available online: [https://oceancolor.gsfc.nasa.gov/reprocessing/r2019/sst/25-Kilpatrick\\_etal\\_GHRSSST\\_XX\\_2019\\_25.jpg](https://oceancolor.gsfc.nasa.gov/reprocessing/r2019/sst/25-Kilpatrick_etal_GHRSSST_XX_2019_25.jpg) (accessed on 1 June 2023).
- NASA/JPL GHRSSST Level 2P Global Sea Surface Skin Temperature from the Moderate Resolution Imaging Spectroradiometer (MODIS) on the NASA Aqua Satellite (GDS2). Available online: [https://podaac.jpl.nasa.gov/dataset/MODIS\\_A-JPL-L2P-v2019.0](https://podaac.jpl.nasa.gov/dataset/MODIS_A-JPL-L2P-v2019.0) (accessed on 1 June 2023).
- NASA/JPL GHRSSST Level 2P Global Sea Surface Skin Temperature from the Moderate Resolution Imaging Spectroradiometer (MODIS) on the NASA Terra Satellite (GDS2). Available online: [https://podaac.jpl.nasa.gov/dataset/MODIS\\_T-JPL-L2P-v2019.0](https://podaac.jpl.nasa.gov/dataset/MODIS_T-JPL-L2P-v2019.0) (accessed on 1 June 2023).

12. Merchant, C.J.; Harris, A.R.; Roquet, H.; Le Borgne, P. Retrieval Characteristics of Non-Linear Sea Surface Temperature from the Advanced Very High Resolution Radiometer. *Geophys. Res. Lett.* **2009**, *36*, L17604. [CrossRef]
13. Petrenko, B.; Ignatov, A.; Kihai, Y.; Stroup, J.; Dash, P. Evaluation and Selection of SST Regression Algorithms for JPSS VIIRS: Selection of SST Regression Algorithms. *J. Geophys. Res. Atmos.* **2014**, *119*, 4580–4599. [CrossRef]
14. ACSPO Global 0.02deg Gridded Super-Collated SST from Low-Earth-Orbiting Platforms (L3S-LEO) | NOAA CoastWatch & OceanWatch. Available online: <https://coastwatch.noaa.gov/cwn/products/acspo-global-002o-gridded-super-collated-sst-and-thermal-fronts-low-earth-orbiting.html> (accessed on 18 July 2023).
15. NOAA In Situ SST Quality Monitor (iQuam). Available online: <https://www.star.nesdis.noaa.gov/socd/sst/iquam> (accessed on 18 July 2023).
16. Johnson, B.T.; Dang, C.; Stegmann, P.; Liu, Q.; Moradi, I.; Auligne, T. The Community Radiative Transfer Model (CRTM): Community-Focused Collaborative Model Development Accelerating Research to Operations. *Bull. Am. Meteorol. Soc.* **2023**, *104*, E1817–E1830. [CrossRef]
17. Liu, Q.; van Delst, P.; Chen, Y.; Groff, D.; Han, Y.; Collard, A.; Weng, F.; Boukabara, S.-A.; Derber, J. Community Radiative Transfer Model for Radiance Assimilation and Applications. In Proceedings of the 2012 IEEE International Geoscience and Remote Sensing Symposium, Munich, Germany, 22–27 July 2012. [CrossRef]
18. JCSDA CRTM (Github). Available online: <https://github.com/JCSDA/crtm> (accessed on 15 September 2023).
19. Cao, C.; Xiong, X.; Wolfe, R.; DeLuccia, F.; Liu, Q.; Blonski, S.; Lin, G.; Nishihama, M.; Pogorzala, D.; Oudrari, H.; et al. Visible Infrared Imaging Radiometer Suite (VIIRS) Sensor Data Record (SDR) User’s Guide Version 1.2. *NOAA Tech. Rep. NESDIS* **2013**, *142*, 43.
20. Xiong, J.; Toller, G.; Sun, J.; Wenny, B.; Angal, A.; Barnes, W. *MODIS Level 1B Algorithm Theoretical Basis Document*; NASA MODIS Characterization Support Team: Washington, DC, USA, 2020.
21. Pytroll/Pyorbital: Orbital and Astronomy Computations in Python. Available online: <https://github.com/pytroll/pyorbital> (accessed on 26 May 2023).
22. OSISAF GHRSSST Level 2P Sub-Skin Sea Surface Temperature from the Advanced Very High Resolution Radiometer (AVHRR) on Metop Satellites (Currently Metop-B) (GDS V2) Produced by OSI SAF. Available online: [http://podaac.jpl.nasa.gov/dataset/AVHRR\\_SST\\_METOP\\_B-OSISAF-L2P-v1.0](http://podaac.jpl.nasa.gov/dataset/AVHRR_SST_METOP_B-OSISAF-L2P-v1.0) (accessed on 14 November 2023).
23. Walton, C.C.; Pichel, W.G.; Sapper, J.F.; May, D.A. The Development and Operational Application of Nonlinear Algorithms for the Measurement of Sea Surface Temperatures with the NOAA Polar-Orbiting Environmental Satellites. *J. Geophys. Res. Oceans* **1998**, *103*, 27999–28012. [CrossRef]
24. Petrenko, B.; Ignatov, A.; Kihai, Y.; Dash, P. Sensor-Specific Error Statistics for SST in the Advanced Clear-Sky Processor for Oceans. *J. Atmospheric Ocean. Technol.* **2016**, *33*, 345–359. [CrossRef]
25. Barton, I.J. Digitization Effects in AVHRR and MCSST Data. *Remote Sens. Environ.* **1989**, *29*, 87–89. [CrossRef]
26. Petrenko, B.; Ignatov, A.; Kihai, Y. Suppressing the Noise in SST Retrieved from Satellite Infrared Measurements by Smoothing the Differential Terms in Regression Equations. In Proceedings of the Volume 9459, Ocean Sensing and Monitoring VII, Baltimore, MD, USA, 21–22 April 2015. [CrossRef]
27. Sun, J.; Wang, M. Electronic Crosstalk in Aqua MODIS Long-Wave Infrared Photovoltaic Bands. *Remote Sens.* **2016**, *8*, 806. [CrossRef]
28. Sun, J.; Madhavan, S.; Xiong, X.; Wang, M. Long-term Drift Induced by the Electronic Crosstalk in Terra MODIS Band 29. *J. Geophys. Res. Atmospheres* **2015**, *120*, 9944–9954. [CrossRef]
29. Xiong, X.; Salomonson, V.V.; Chiang, K.-F.; Wu, A.; Guenther, B.W.; Barnes, W. On-Orbit Characterization of RVS for MODIS Thermal Emissive Bands. In Proceedings of the Volume 5652, Passive Optical Remote Sensing of the Atmosphere and Clouds IV, Honolulu, HI, USA, 9–10 November 2004. [CrossRef]
30. NOAA STAR SST Team. ACSPO Regional Monitor (ARMS). Available online: <https://www.star.nesdis.noaa.gov/socd/sst/arms> (accessed on 19 July 2023).
31. Bouali, M.; Ignatov, A. Reduction of Stripe Noise in ACSPO Clear-Sky Radiances and SST. In Proceedings of the Volume 8724, Ocean Sensing and Monitoring V, Baltimore, MD, USA, 29 April–3 May 2013. [CrossRef]
32. Gladkova, I.; Ignatov, A.; Shahriar, F.; Kihai, Y.; Hillger, D.; Petrenko, B. Improved VIIRS and MODIS SST Imagery. *Remote Sens.* **2016**, *8*, 79. [CrossRef]
33. Minnett, P.J.; Alvera-Azcárate, A.; Chin, T.M.; Corlett, G.K.; Gentemann, C.L.; Karagali, I.; Li, X.; Marsouin, A.; Marullo, S.; Maturi, E.; et al. Half a Century of Satellite Remote Sensing of Sea-Surface Temperature. *Remote Sens. Environ.* **2019**, *233*, 111366. [CrossRef]
34. NOAA STAR SST Team. SST Quality Monitor (SQUAM). Available online: <https://www.star.nesdis.noaa.gov/socd/sst/squam> (accessed on 21 September 2023).
35. JPSS GS Systems Engineering Joint Polar Satellite System (JPSS) Ground Segment Data Product Specification (GSegDPS), 474-01543, Revision A 2019. Available online: [http://www.nesdis.noaa.gov/s3/2022-03/474-01543\\_JPSS-GSegDPS\\_A.pdf](http://www.nesdis.noaa.gov/s3/2022-03/474-01543_JPSS-GSegDPS_A.pdf) (accessed on 28 November 2023).
36. Merchant, C.J.; Embury, O.; Rayner, N.A.; Berry, D.I.; Corlett, G.K.; Lean, K.; Veal, K.L.; Kent, E.C.; Llewellyn-Jones, D.T.; Remedios, J.J.; et al. A 20 Year Independent Record of Sea Surface Temperature for Climate from Along-Track Scanning Radiometers: SST for Climate From ATSRs. *J. Geophys. Res. Oceans* **2012**, *117*, C12. [CrossRef]

37. CMC L4 0.1deg Global Foundation Sea Surface Temperature Analysis (GDS Version 2). Available online: <https://podaac.jpl.nasa.gov/dataset/CMC0.1deg-CMC-L4-GLOB-v3.0> (accessed on 14 December 2021).
38. Wong, A.; Keeley, R.; Carval, T.; Argo Data Management Team. *Argo Quality Control Manual for CTD and Trajectory Data*; Ifremer: Plouzané, France, 2021. [CrossRef]
39. Cleveland, R.B.; Cleveland, W.S.; McRae, J.E.; Terpenning, I. STL: A Seasonal-Trend Decomposition Procedure Based on Loess (with Discussion). *J. Off. Stat.* **1990**, *6*, 3–73.
40. Xiong, X.; Aldoretta, E.; Angal, A.; Chang, T.; Geng, X.; Link, D.; Salomonson, V.; Twedt, K.; Wu, A. Terra MODIS: 20 Years of on-Orbit Calibration and Performance. *J. Appl. Remote Sens.* **2020**, *14*, 1. [CrossRef]
41. Xiong, X.; Wu, A.; Wenny, B.N.; Madhavan, S.; Wang, Z.; Li, Y.; Chen, N.; Barnes, W.; Salomonson, V. Terra and Aqua MODIS Thermal Emissive Bands On-Orbit Calibration and Performance. *IEEE Trans. Geosci. Remote Sens.* **2015**, *53*, 5709–5721. [CrossRef]
42. MCST: Terra Spacecraft and MODIS Instrument Status. Available online: <https://mcst.gsfc.nasa.gov/terra-spacecraft-and-modis-instrument-status> (accessed on 19 July 2023).
43. CMC L4 0.2deg Global Foundation Sea Surface Temperature Analysis (GDS Version 2). Available online: <http://podaac.jpl.nasa.gov/dataset/CMC0.2deg-CMC-L4-GLOB-v2.0> (accessed on 14 December 2021).
44. Global Modeling and Assimilation Office (GMAO) MERRA-2 inst3\_3d\_asm\_Np: 3d, 3-Hourly, Instantaneous, Pressure-Level, Assimilation, Assimilated Meteorological Fields V5.12.4. Available online: [https://disc.gsfc.nasa.gov/datasets/M2I3NPASM\\_5.12.4/summary](https://disc.gsfc.nasa.gov/datasets/M2I3NPASM_5.12.4/summary) (accessed on 15 September 2023).
45. Global Modeling and Assimilation Office (GMAO) MERRA-2 inst1\_2d\_asm\_Nx: 2d,1-Hourly, Instantaneous, Single-Level, Assimilation, Single-Level Diagnostics V5.12.4. Available online: [https://disc.gsfc.nasa.gov/datasets/M2I1NXASM\\_5.12.4/summary](https://disc.gsfc.nasa.gov/datasets/M2I1NXASM_5.12.4/summary) (accessed on 15 September 2023).
46. Gelaro, R.; McCarty, W.; Suárez, M.J.; Todling, R.; Molod, A.; Takacs, L.; Randles, C.A.; Darmenov, A.; Bosilovich, M.G.; Reichle, R.; et al. The Modern-Era Retrospective Analysis for Research and Applications, Version 2 (MERRA-2). *J. Clim.* **2017**, *30*, 5419–5454. [CrossRef]
47. NOAA ACSPO v2.80 NPP VIIRS L2P SST. Available online: [https://podaac.jpl.nasa.gov/dataset/VIIRS\\_NPP-STAR-L2P-v2.80](https://podaac.jpl.nasa.gov/dataset/VIIRS_NPP-STAR-L2P-v2.80) (accessed on 31 January 2022).
48. Embury, O.; Bulgin, C.E.; Mittaz, J. ESA Sea Surface Temperature Climate Change Initiative (SST\_cci): Along-Track Scanning Radiometer (ATSR) Level 2 Preprocessed (L2P) Climate Data Record, Version 2.1. Available online: <https://catalogue.ceda.ac.uk/uuid/916b93aaf1474ce793171a33ca4c5026> (accessed on 15 May 2023).
49. Merchant, C.J.; Embury, O.; Bulgin, C.E.; Block, T.; Corlett, G.K.; Fiedler, E.; Good, S.A.; Mittaz, J.; Rayner, N.A.; Berry, D.; et al. Satellite-Based Time-Series of Sea-Surface Temperature since 1981 for Climate Applications. *Sci. Data* **2019**, *6*, 223. [CrossRef] [PubMed]
50. Roemmich, D. The Argo Steering Team. *Oceanography* **2009**, *22*, 46–55. [CrossRef]
51. MCST: MODIS Blackbody Warmup/Cooldown Events. Available online: <https://mcst.gsfc.nasa.gov/modis-events-categories/bb-warmupcooldown> (accessed on 19 July 2023).

**Disclaimer/Publisher’s Note:** The statements, opinions and data contained in all publications are solely those of the individual author(s) and contributor(s) and not of MDPI and/or the editor(s). MDPI and/or the editor(s) disclaim responsibility for any injury to people or property resulting from any ideas, methods, instructions or products referred to in the content.